HYDROTHERMAL SYNTHESIS AND CHARACTERIZATION OF SINGLE CRYSTALLINE CeO_2 NANOPARTICLES FOR CATALYTIC APPLICATIONS

A Thesis Submitted to
the Graduate School of Engineering and Sciences of
İzmir Institute of Technology
in Partial Fulfillment of the Requirements for the Degree of

MASTER OF SCIENCE

in Chemistry

by
Taylan MEŞİN

July 2012
İZMİR

We approve the thesis of **Taylan MEŞİN**

Examining Committee Members:

_____

Assoc. Prof. Dr. Funda DEMİRHAN
Department of Chemistry, Celal Bayar University

_____

Assoc. Prof. Dr. Mustafa M. DEMİR
Department of Chemistry, İzmir Institute of Technology

_____

Assist. Prof. Dr. Mustafa EMRULLAHOĞLU
Department of Chemistry, İzmir Institute of Technology

09 July 2012

_____

Assoc. Prof. Dr. Mehtap EMİRDAĞ EANES
Supervisor, Department of Chemistry,
İzmir Institute of Technology

_____

Assist. Prof. Dr. Ali ÇAĞIR
Co-supervisor, Department of Chemistry, İzmir Institute of Technology

_____

Prof. Dr. Durmuş ÖZDEMİR
Head of the Department of Chemistry

_____

Prof. Dr. R. Tuğrul SENGER
Dean of the Graduate School of Engineering and Sciences

ACKNOWLEDGEMENTS

I will first and foremost like to thank my great supervisor Assoc. Prof. Mehtap EMİRDAG EANES who has supported me throughout my thesis with her endless patience. Whenever I had a problem, she always gave me her valuable advices. One simply could not wish for a better or friendlier supervisor.

Also, I would like to appreciate deeply my co-supervisor Assist. Prof. Dr. Ali Çağır for his kind support, valuable comments and understanding.

Next, I want to thank Clemson University of Materials Research for Transmission Electron Microscope images and Center (IYTE MAM) for Scanning Electron Microscope and X-ray Diffraction analysis.

Additionally, I would like to thank my dearest friend Doğan TAÇ for his encouragement and never ending friendship. Whatever obstacles I come across, he always find a solution. I owe him so much.

Special thanks to all my friends in IZTECH especially Banu ÖNEN, Merve DEMİRKURT, Esen DÖNERTAŞ, Melih KUŞ, Fırat ZİYANAK, Muhammed ÜÇÜNCÜ, Mithat BOZ and Erman KARAKUŞ.

Finally, my deepest gratitude goes to my precious girlfriend Leyla ÖZTÜRK for her endless love, understanding and encouragement throughout my entire life. It would not be possible to complete this thesis without her support.

Dedicated to;

my lovely family for being with me in all my life…

ABSTRACT

HYDROTHERMAL SYNTHESIS AND CHARACTERIZATION OF SINGLE CRYSTALLINE CeO_2 NANOPARTICLES FOR CATALYTIC APPLICATIONS

Single crystalline cerium oxide nanoparticles were synthesized with hydrothermal method by mixing cerium nitrate [$Ce(NO_3)_3.6H_2O$] aqueous solution with alkali bases CsOH and RbOH. SEM, TEM and XRD characterization methods were used in order to identify morphology.

First part of the study includes the work on effect of hydrothermal parameters, such as reaction temperature, reaction time, alkali base type and concentration on particle size and morphology. It was prooved that the size of ceria nanoparticles is directly proportional with the reaction time. The reaction temperature is also an important parameter that effect the morphology of nanoparticles. At 120 ^oC nanoparticles form rod like structure and as time goes they start to form cubic crystals. When the alkali base and concentration was changed the results showed that higher base concentration favors the particles to form bigger structures than that of lower concentrations. In addition, optical properties of CeO_2 nanoparticles were studied by using the UV-Vis and Fluorescence Spectrometry. UV-Vis Spectroscopy results show that particle size of CeO_2 nanoparticles synthesized in the presence of 8M RbOH are larger than that of synthesized in presence of 8M CsOH. When the reaction time decreases the Ce^{3+} defect increases based on the results of Fluorescence Spectrometry results.

Second part of the study includes catalytic property of CeO_2 nanoparticles. Ceria nanoparticles were used as catalyst in the synthesis of flavone from 2'-hydroxychalcone. Several reaction parameters were studied in order to achieve the flavone synthesis. TLC, GC, GC-MS and NMR were used in order to monitor the results of the reactios.

ÖZET

KATALİTİK UYGULAMALAR İÇİN TEK KRİSTAL CeO_2 NANOPARÇACIKLARININ HİDROTERMAL SENTEZİ VE KARAKTERİZASYONU

Tek kristal seryum oksit nanoparçacıkları Seryum nitratın [$Ce(NO_3)_3.6H_2O$] CsOH ve RbOH alkali bazlarının sulu çözeltilerinin hazırlanmasının ardından hidrotermal metot ile sentenzelenmiştir.Taramalı ve geçirimli elektron mikroskopu ve X-ray kırınımı yöntemleri kullanılarak parçacıkların morfoloji ve kristal özellikleri saptanmıştır.

Çalışmanın ilk kısmı reaksiyon zamanı, reaksiyon sıcaklığı, alkali baz çeşidi ve konsantrasyonu gibi parametrelerin değişiminin paraçacık boyutuna ve morfolojisine olan etkilerini içermektedir. Sonuçlara bakıldığında açıkça söylenebilir ki reaksiyon süresiyle parçacık boyutu doğru orantılı bir şekilde artım göstermiş olup reaksiyon süresi arttığında topaklanmanın yerini homojen dağılım almıştır. Reaksiyon sıcaklığıyla ilgili yapılan denemelerde 120 ^oC de sentezlenen nanoparçacıkların çubuk şeklinde olduğu, sıcaklık arttıkça kübik bir yapıya dönüştüğü gözlemlenmiştir. Ayrıca baz konsantrasyonunun artışıda parçacıkların büyümesinde etkili bir rol oynamıştır. Bu çalışmalara ilaveten UV-Vis spektrometri ve Florasans Spektrometri cihazları kullanılarak seryum oksit nanoparçacıklarının optik özellikleri araştırılmış olup UV-Vis spektrum sonuçlarından yola çıkılarak RbOH alkali bazıyla sentezlenen nanoparçacıkların CsOH ile sentezlenenlerden daha büyük olduğu tayin edilmiştir. Floresans sonuçlarında ise reaksiyon zamanı azalımının kristal kusurlarını azaltığı gözükmektedir.

Son kısımda ise CeO_2 nanoparçacıklarının katalitik özellikleri araştırılmaya çalışılmıştır. Nanoparçacıklar 2'-hidroksiçalkondan flavon maddesinin sentezlenmesinde katalizör olarak kullanılmıştır. Sentezi tamamlamak için çözgen, reaksiyon sıcaklığı, nanoparçacık çeşidi ve kullanılan baz gibi parametreler değiştirilmiş, ürün oluşumu GC, GC-MS ve TLC ile takip edilmiş, son ürün NMR ile karakterize edilmiştir.

TABLE OF CONTENTS

LIST OF FIGURES

LIST OF TABLES

CHAPTER 1

INTRODUCTION

Nanotechnology is a field, deals with every branch of science such as biology, chemistry, physics and enginering subjects. Between 100 nm and few nanometers is the field of nanotechnology study. Origin of ‘nano’ is the Greek word of nanos which means ‘dwarf’. This prefix is used in the metric system to mean 10-9 or one billionth (1/1,000,000,000).

In general although its main definition is known as technology of fabrication, design, characterization and application of structures devices and systems by controlling shape and size at nanometer scale, it is also portraited as towards to nano scale component of materials and systems show significant improvement in their physical, biological and chemical properties and processes.

There are several fabrication methods for nanomaterials such as top-down, bottom-up and mixed methods. Top-down chemical fabrication methods are always easy to upscale and many are widespread industrial areas. Bulk material is the starting material for top-down method in order to form nano materials. Top-down methods include mechanical, thermal, high-energy, chemical and other techniques. Various examples of top-down methods are: mechanicanosynthetic methods, thermal methods, high energy methods, lithographic methods.

For bottom-up method, an atom or a molecule is the starting material to build nano materials by addition of substances also bottom-up liquid phase methods are the primary vehicle for self-assembled systems. CVD (chemical vapor deposition), MOCVD (metal-organic chemical vapor deposition), ALD (atomic layer deposition) gas-phase methods are included in bottom-up method. Various examples of bottom-up methods are chemical vapor deposition method, atomic layer deposition methods, metal-organic chemical vapor deposition methods, liquid phase methods methods, electrodeposition and electroless deposition methods (Nanoscienceworks 2012).

Quantum effects start to predominate in nanometer size range that provides nano particles to have high surface area to volume ratio. The relationship between surface area and particle size is inversially proportional with each other. As particle size decreases the surface to volume ratio increases. The relation can be seen in Figure 1.1.

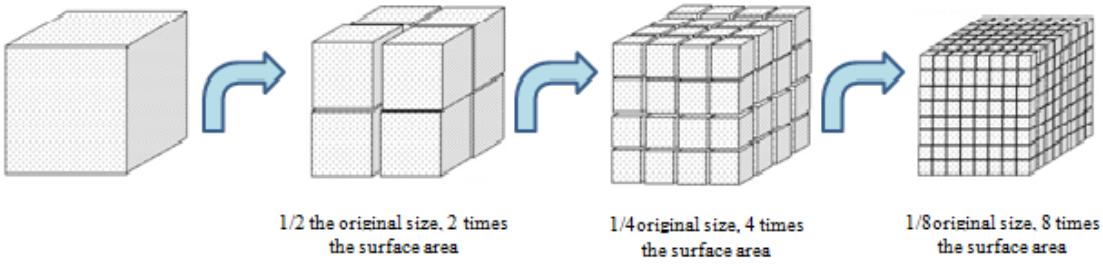

Figure 1.1. Particle size-surface area relationship.

As it mentioned when the particle size decreases, the surface area increases. Higher surface area also means higher surface energy that is very beneficial for catalytic processes but high surface energies make nanomaterials thermodynamically unstable. To achieve this situation there are some methods that gather small particles to form larger ones in order to decrease surface energy. Some methods are sintering process and Ostwald ripening process. At sintering process small particles gather to form larger ones but in Ostwald process expension of small particles form large ones. Main difference between these processes is the temperature range that is necessary to complete the process. In sintering low temperatures including room temperature is neglited and give significant results at high temperatures (70% of particles melting point), in Ostwald process it is easy to work with wide range of temperature also at low temperatures. Low temperatures provide nanoparticles to disperse and to gain solubility in a solvent. (Kang 2005).

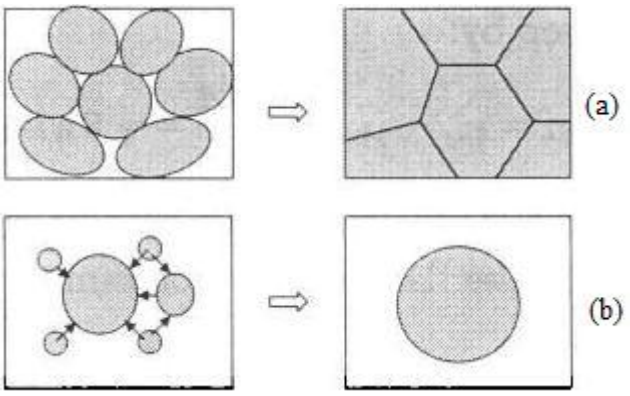

Figure 1.2. Illustration of sintering (a) and Ostwald process (b)
(Source: Cao 2004)

1.1. Cerium Oxide Nanoparticles

With the development of the researches in nanostructured materials, Cerium oxide (CeO_2) nanoparticles have been extensively studied over the last two decades. Cerium oxide also known as cerium dioxide and ceria. It is pale yellow color as shown in Figure 1.3.

In periodic table, ceria is located at lanthanoids part and has the $4f^2 6s^2$ electron configuration. It shows both Ce+3 and Ce+4 electron configuration. Cerium is reduced to CeO_2 and Ce_2O_3 in the presence of oxygen. Ce_2O_3 is the +3 configuration of cerium and has yellow green pulver color. Cerium oxide has the same structure with fluorite (face centered cubic unit cell). Cell parameter of this structure is 5.410 Å (Space group Fm3m, JCPDS 81-0792). Some important physical and chemical characteristics of bulk CeO_2 was shown in Table 1.1.

Figure 1.3. Cerium oxide powder.

Table 1.1. Some important physical and chemical characteristics of bulk CeO_2 (Source: Integrated Laboratory Systems, Inc. 2006).

	Cerium Oxide
Formula	CeO_2
Molecular Weight	172.12 g/mol
Physical State	Solid, cubic, face-centered crystals. Solid as white, yellow or tan powders
Density	7.65 g/cm^3
Boiling Point	Not available (melts at 2500°C–2600°C)
Water Solubility	Not soluble
Refractive Index	2.0
Hardness	5–6

As it mentioned CeO_2 has the fluorite structure that consists of cubic close-packed array of metals with all tetrahedral holes filled by oxygen that is illustrated in Figure 1.4. When cerium oxide is treated at elevated temperatures in reducing athmosphere CeO_2 forms non-stoichiometric CeO_{2-X} ($0 < x < 0.5$) oxides. Although it losts oxygen from its lattice, CeO_2 remains in its structure and suboxidized cerium oxides' reoxidized to CeO_2 in oxidizing medium (Trovarelli 2006).

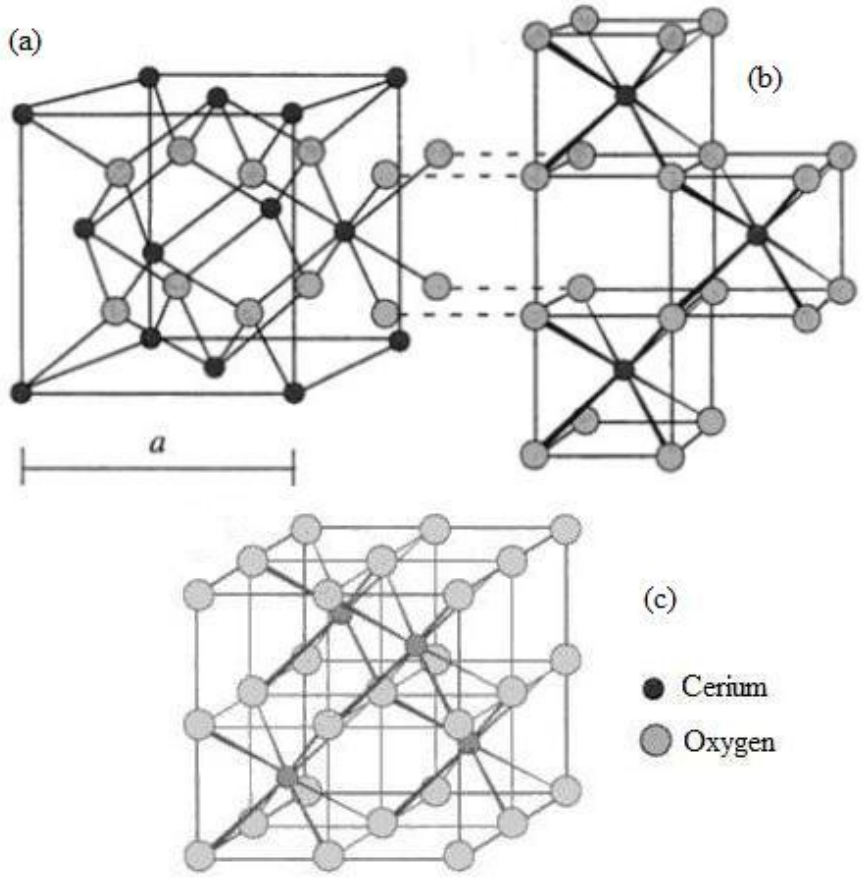

Figure 1.4. Crystal structure of cerium oxide (a) unit cell as a *ccp* array of cerium atoms and (b) and (c) the same structure redrawn as a primitive cubic array of oxygen ions (Source: Trovarelli 2002).

1.2. Applications of Cerium Oxide Nanoparticles

Cerium oxide is widely known as its oxygen storage capacity and high oxygen ion conductivity (Campbell and Peden 2005). Cerium oxide nanoparticles are used as polishing powders (Kosynkin, et al. 2000), gas sensors (Khodadadi, et al. 2001), UV-blockers (Imanaka, et al. 2003) and catalyst. There are several catalytic studies with cerium oxide nanoparticles in literature. In 2003 Rao, et al. converts harmful hydrocarbons, carbon monoxide and nitrogen oxides in to hydrogen, nitrogen and water by the help of cerium oxide nanoparticle catalysis (Rao, et al. 2003). Wang and Lin incinerate toluene in to water and carbon dioxide by using different sized cerium oxide nanoparicles as a catalyst (Wang, et al. 2004).

1.3. Chalcones

Chalcones and its derivatives are aryl styryl ketones. They are the class of flavanoid family. They show important biological activities such as; anti-cancer, anti-bacterial and anti-oxidant. The source of chalcones are plants and they are produced by biosynthetic pathways. In literature there are many studies about the isolation of chalcones from natural sources (Adesanwo, et al. 2009, Van Puyvelde, et al. 1989).

Chalcones can be synthesized by aldol reaction of corresponding aldehyde and ketone under both acidic or basic medium. $AlCl_3$ (Calloway and Green, 1937), $RuCl_3$ (Ironpoor and Kazemi, 1998), ant $TiCl_4$ (Mazza and Guaram, 1980) are the few examples of these acid catalyst. Also chalcones are synthesized by Claisen-Schmidt reaction catalyzed by strong base like NaOH or KOH (Kazauki, et al. 1976). In this study commercialy available 2'-hydroxychalcone shown in Figure 1.5 was used as a precursor for the synthesis of corresponding flavones.

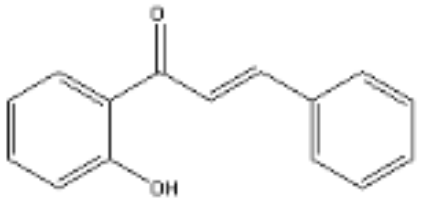

1

Figure 1.5. Structure of 2'-hydroxychalcone

1.4. Flavanones

Flavanones **(2)** are another subclass of flavanoids, formed by biotransformations of 2'-hydroxychalcones **(1)** via chalcone-flavanone isomerase enzyme, possesing strong anti-oxidant activity. Syntheticaly Flavanones are generally prepared by Michael addition type cyclization of 2-hydroxychalcones **(1)** as in Figure 1.6.

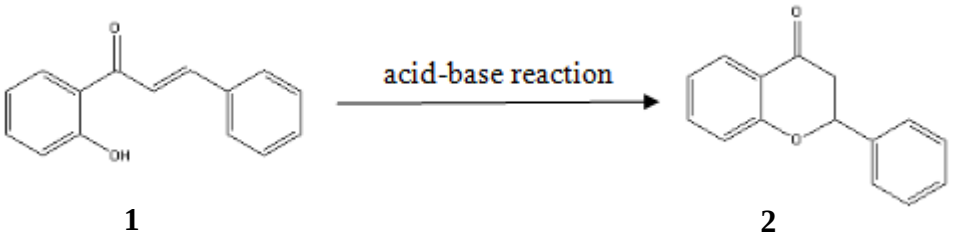

1 **2**

Figure 1.6. Michael addition type cyclization of 2'hydroxychalcone **(1)**

Cyclization reaction can be done under both acidic or basic catalyst.Transformation of 2'-hydroxychalcone **(1)** to flavanone **(2)** by refluxing in glacial acetic acid is an example of acid catalized cyclization method (Cabrera, et al. 2007).

1.5. Flavones

Flavones are the class of flavanoids. It is based on the backbone of 2-phenylchromen-4-one (2-phenyl-1-benzopyran-4-one) shown on Figure 1.7.

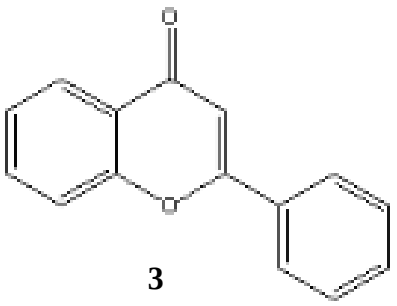

3

Figure 1.7. Structure of flavone

Apigenin, Luteolin, Tangeritin, Chrysin, Baicalein, Scutellarein, Wogonin are exmples of natural flavones. Diosmin and Flavoxate are synthetic types of flavones. For several years interest on flavones have been increased due to their beneficial effects against asteoporosis, diabetes, atherosclerosis and certain cancers (Cermak 2008).

There are several synthesis methods for flavones: Allan-Robinson reaction (Dyke, et al. 1961), Auwers synthesis (Auwers 1908), and the Algar-Flynn-Oyamada reaction (Gormleg, et al 1973). In this study flavones **(3)** are tried to produced firstly by

producing flavanone **(2)** from 2'-hydroxychalcone **(1)** and then oxidation reaction by cerium oxide nanoparticle catalyst.

1.6. Synthesis Methods

Cerium oxide nanoparticles are synthesized by various methods such as hydrothermal, solvothermal, chemical precipitation, sol-gel and microemulsion (reverse micelles) methods. Recently, Sathyamurth, et al. (2005) succeeded to synthesize with an average of 3.7 nm sized cerium oxide nanoparticles by microemulsion method, Yin, et al. (2002), produced approximately 4 nm cerium oxide nanoparticles by sonochemical synthesis, according to Han, et al. (2005), they produced nanowires and nanotubes with hydrothermal synthesis and Zhou, et al. (2002), synthesized 4 nm of cerium oxide nanoparticles by precipitation method.

1.6.1. Sol-gel Synthesis

Sol-gel method is one of the most applied method for synthesizing nanomaterials. The basis of this method is the phase transformation of a sol obtained from organometallic precursors and metallic alkoxides. This sol contains particles in suspension and it is polimerized at low temperatures then it forms wet gel. The last step of this technique is drying the gel to prevent the solvent and heating properly. Figure 1.8 shows the schematic route of sol-gel process.

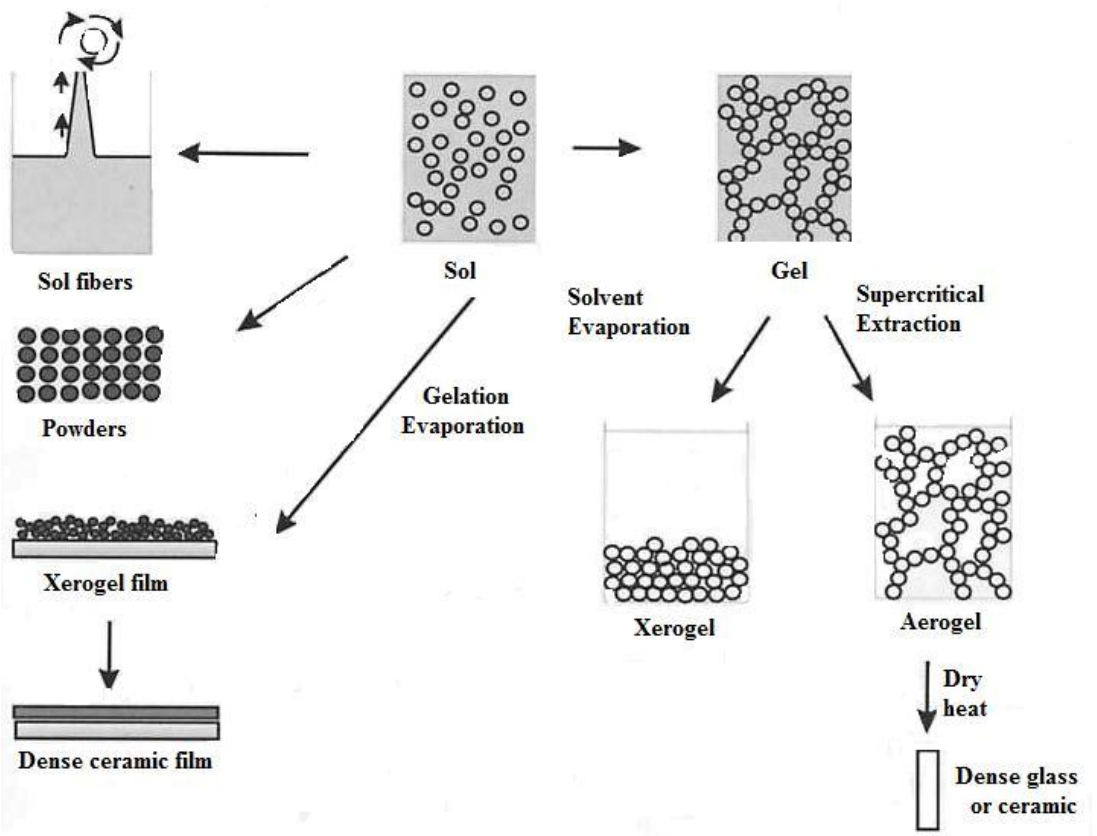

Figure 1.8. Sol-gel processing options
(Source: Schubert and Hüsing 2000).

Genaraly alkoxides are used as a starting precursor but some sol-gel processes do not need alkoxides. Wu, et al. (2004) used porous anodic alumina template (PAA) instead of alkoxides and succeeded to produce CeO_2 nanowires.

1.6.2. Synthesis in Microemulsion (Reverse Micelles)

With the development of the microemulsion method, it becomes appropriate way to synthesize nanocrystals with controlled size and surface (Zhang, et al. 2001). In microemulsion method the latter is thermodynamically and the former is kinetically stable. Temperature changes, pressure and additives change the stability (Paul and Moulik 2001).

Microemulsions which were illustrated in Figure 1.9. are classified in to three (Winsor 1948);

1) The surfactant is soluble in water and oil in water (o/w) microemulsions (micelles)
2) The surfactant is in the oil and water in oil (w/o) microemulsions (reverse micelles)
3) In this type surfactant rich midle phase, excess water and oil surfactant poor phase forms three phases (o+w).

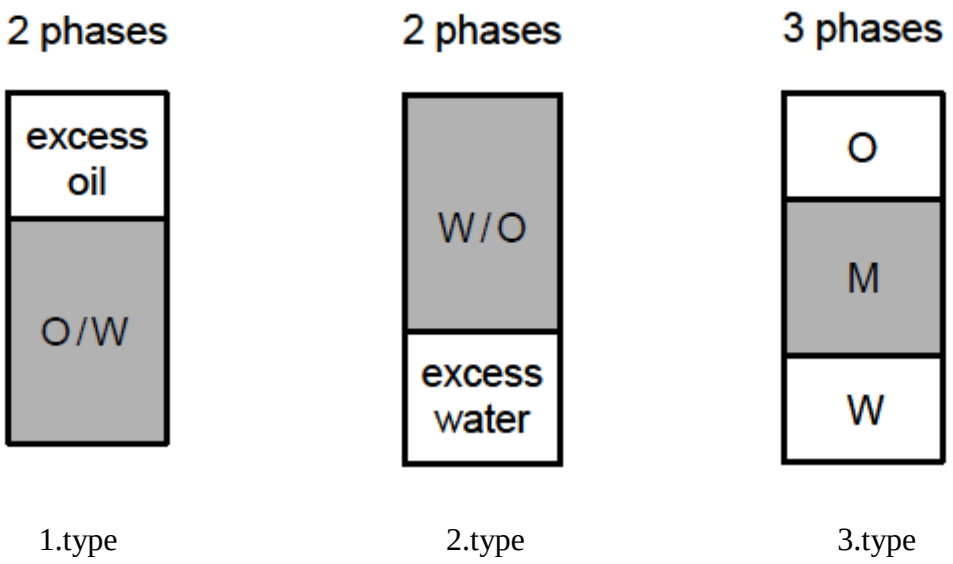

Figure 1.9. Microemulsion types.

Sathyamurth, et al. Produced cerium oxide nanoparticles with this method. Their system consists cerium nitrate and NaOH as precursors, octane instead of oil phase and cetyl trimethyl ammonium bromide (CTAB) as a surfactant. The scheme of the system is illustrated in Figure 1.10. They succeeded to produce 3.7 nm sized cerium oxide nanoparticles (Sathyamurth, et al. 2005).

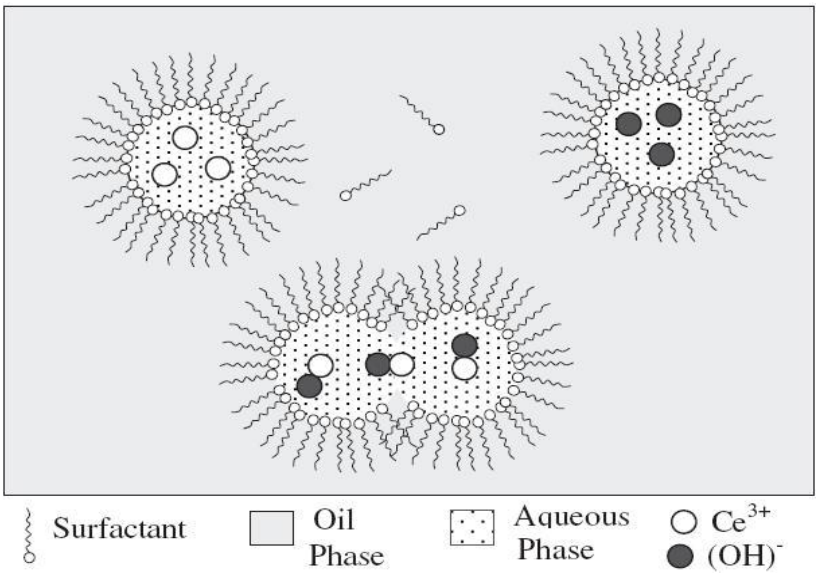

Figure 1.10. Illustration of nanoparticle synthesis using reverse micellar synthesis. (Source: Sathyamurthy, et al. 2005).

1.6.3. Chemical Precipitation Method

A solid substance is formed with chemical precipitation method. Chemical reaction, nucleation and crystal growth are the three steps of this method. Xiandong, Feng and Michael pointed out the disadvantages of this method. The handicap of this process is having a wide size distribution of particles. Additionally wide size distribution, agglomeration and uncontrolled particle morphology problems should be taken into consedaration while applying chemical precipitation method.

A solution containing metal cations are added to oxide powders in order to form precipitate in procedure. In order to prevent the problems, homogeneous precipitation method has been developed. In this process, precipitating ligands from another chemical source of the solution are released to generate precipitants throughout the solution. In 1993 Chen, et al. used hexamethylenetetramine (HMT) and urea. They yield amonia by decomposing at about 70-80^{o}C. Figure 1.11. shows the spherical CeO_2 nanoparticles synthesized with this method (Chen and Chen 1993).

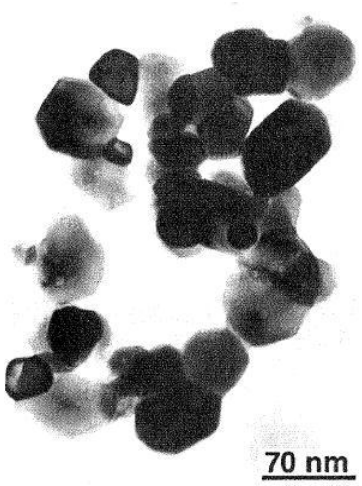

Figure 1.11. TEM image of powders prepared with Ce-HMT calcined at 450°C.
(Source: Chen and Chen 1993)

1.6.4. Hydrothermal Synthesis

1.6.4.1 History of Nanomaterial Process with Hydrothermal Synthesis

For nearyl quarter decade hydrothermal synthesis has been very popular technique and gained interest. In the 18th century British geologist Sir Roderick Murchison firstly used hydrothermal technique. The aim was to define earths' erust changes. Also rock and mineral formation was monitored by the action of water at elevated temperature and pressure. Then in 2001 Byrappa and Yoshimura developed hydrothermal technique to achieve the mineral formation more obvious to understand.

In 1845, the first attempt of hydrothermal synthesis for nanomaterials was carried out by Schaufthaul. Between 1840s and early 1900s lots of nanomaterial synthesis experiments were done via hydrothermal synthesis techniques but there was a handicap in those days that there weren't any microscipic techniques exist (Byrappa and Adschiri). Commercialy Karl Josef Bayer (1892) took the first step by synthesizing pure aluminum hydroxide which was easy to convert into pure Al_2O_3 (Goranson 1931). Nacken (1946) followed Bayer by synthesizing large single crystals and Barrer (1948) for zeolites (Nacken 1946, Barer 1948).

Lack of knowledge on hydrothermal solution chemistry and kinetics of hydrothermal reactions failed crystalline materials to be analyzed between the late

1920s and late 1950s. With the first high resolution scaning electron microscope, fine crystal analysis started. Scientists increased their interest to this technique on nanostructured materials because it provides coating various materials on metals, polymers, etc. In these days hydrothermal synthesis technique can be applied by chemists, biologists, physicist, geologists and engineers. Figure 1.12. shows the wide variety usage areas of hydrothermal synthesis (Byrappa and Adschiri 2007).

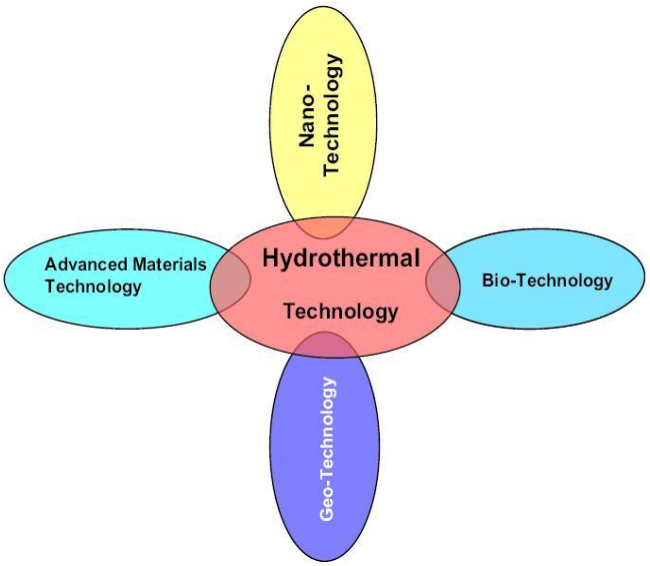

Figure 1.12. In 21st century, illustration of hydrothermal technology
(Source: Byrappa and Adschiri 2007).

1.6.4.2. Definition and Process of Hydrothermal Synthesis

Principally, hydrothermal means that making insoluble materials under normal conditions dissolve and recrystallize with high temperature and pressure in presence of aqueous solvent or mineralizers.The word “hydrothermal” comes from Grecian which is combining two words Hydros (water) and thermos (heat) (Byrappa and Adschiri 2007). There are several approaches for hydrothermal synthesis in the literature.For example, Laudise explains that hydrothermal synthesis is the growth from aqueous solution at ambient conditions (Laudise 1970). Rabenau describes that more specificly as it is the heterogeneous reactions in aqueous media above 100 °C and 1 bar (Rabenau 1985). Most lately approach is defined by Roy. According to Roy using water as a catalyst and rarely as a component of solid phases at temperatures more than 100 °C

and pressures greater than 1 atm is the hydrothermal synthesis (Roy 1994). After Roy, Yoshimura tried that reactions under high temperatures and pressures (>100°C and >1 atm) in a closed system.

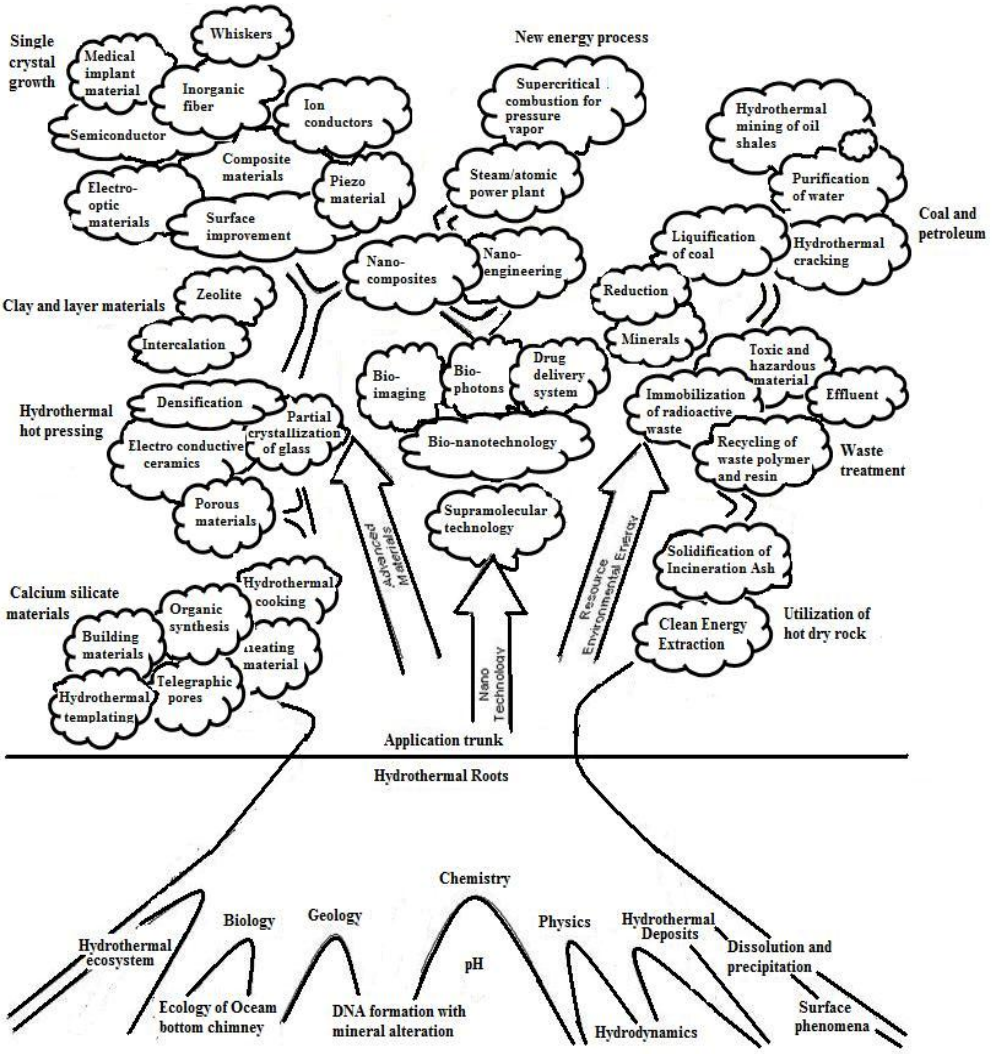

Figure 1.13. Hydrothermal tree showing different branches of science and technology (Source: Byrappa and Adschiri 2007).

Common opinion of scientists is the hydrothermal synthesis is occured above 100 °C and above 1 atm. At the same time there is no lower limit for pressure and temperature conditions. Thus, hydrothermal synthesis is more accurately defined as heterogeneous chemical reaction with water existance above room temperature and 1 atm in a closed vessel (Byrappa and Adschiri 2007).

Occasionally solvothermal terminology is used instead of hydrothermal

terminology when a solvent is another material. Also different names are used depend on the solvent type as glycothermal, ammonothermal, alcohothermal and etc. On the other hand,using water as a solvent gives some advantages like minimizing pollution because water is easily volatilized and can be recycled (Komarneri 2003). In addition that there are environmental benifits and water is cheaper than the other solvents. Water can pretend like a catalyst for transformation of desired materials when the temperature and pressure are adjusted properly (Byrappa and Yoshimura 2001). Under hydrothermal conditions, it is hard to dissolve some reactants in water and this handicap can be removed by supplementing mineralizers or solvents. Mineralizers quicken the reaction rate and crystal formation. They provide to raise ability of the compound solubility in water. The hydroxides of alkali metal salts like NaOH, KOH or LiOH, alkali salts of weak acids or elemental acids are used as mineralizers.

Pressure-temperature relations of water is very important for hydrothermal syntheses in closed vessel with constant volume. Figure 1.14. represents the volume-temperature diagram of water. In this diagram, volume is replaced with density. Two-phase region which the liquid and gas phases are at equilibrium is illustrated in diagram. Density of two phases is determined by the intersections of a horizontal line at a given temperature. At 300 °C, the density is 0.75 g/cm^3 for liquid phase and 0.05 for gas phase for an illustration. Density of liquid phase decreases with increasing temperature, however, density of gas phase increases. Temperature and density of these two phases are at equilibrium at critical point. That means above the critical point there is only one phase is present. That is called “supercritical or fluid phase” (Schubert and Hüsing 2000).

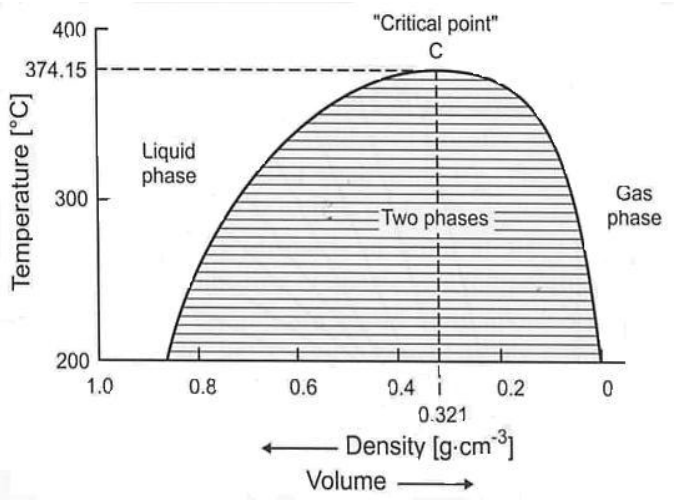

Figure 1.14. Volume (density)/temperature dependence of water
(Source: Schubert and Hüsing 2000)

All pressure values are self-generated in which the internal expansion of a fluid with presure that is produced by heating without any external factors during the synthesis. The fluid expands quickly to fill the teflon container at the reaction temprature when it is put in a container at low temperature. In this section filling temperature is the key parameter and this parameter is the determination point for ultimate pressure from the initial room temperature fill.This can be evaluated by using pressure-temperature (P-T) tables which is shown on Figure 1.15. On this figure T_r represents triple point (solid-liquid-gas phases coexist) and C represents critical point.

In general, initially fills are founded more than 32% then the liquid begins to fill the whole autoclave at temperatures below critical point (373 °C) because high temperature causes to raise the meniscus between gas and liquid phase. For example, when the initial rate of filling is 80%, the autoclave is filled fully at below the critical temperature approximately 245 °C. Liquid level remains same till reaching critical temperature if autoclave is filled 32% exactly. If the filling rate less than 32%, it cause to decreas of the level of liquid and below critical temperature one phase coexist that is gas phase (Schubert and Hüsing 2000). As general, when the percentage of filling increases, the temperature of autoclave filling with water decreases.

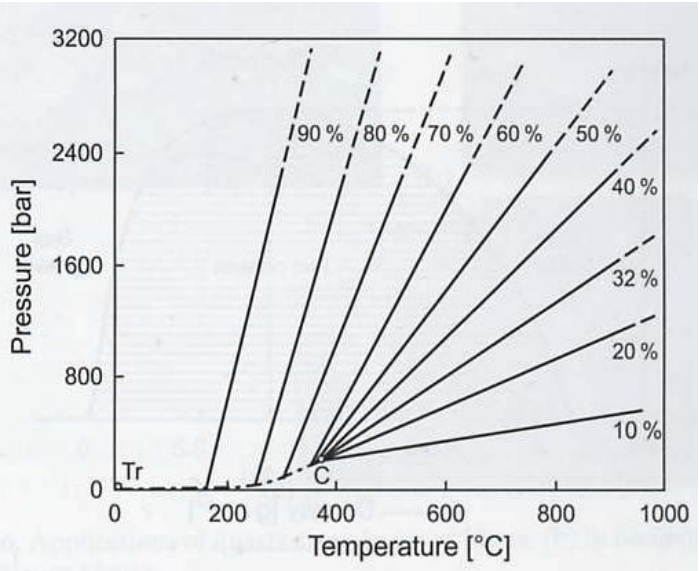

Figure 1.15. PT dependence of water for different degrees of filling of the vessel (Source: Schubert and Hüsing 2000).

In conclusion, hydrothermal technique gives some extra benifits if it is compared to conventional synthesis techniques. Firstly, even at low temperatures, desired crystalline materials can be directly synthesized and like in sol-gel processing calcination step do not require. In addition to this, it is easy to control particle size and morphology in hydrothemal synthesis by changing the conditions like pH, temperature or nature of surfactant. At last, resulting materials can be used directly in steps like filtration (Kaya, et al. 2002).

1.7. The Purpose of the Study

The purpose of this study is to synthesize cerium oxide (CeO_2) nanoparticles with hydrothermal method and determine the effects of alkali type, alkali concentration, reaction time and reaction temperature on structure and particle size. Then the optical and catalytic properties of CeO_2 nanoparticles are determined.

CHAPTER 2

EXPERIMENTAL METHODS

2.1. Reaction Autoclaves

Hydrothermal conditions reactions require a closed vessel that is durable to high temperatures and pressures. This closed vessel is named as an autoclave and an ideal autoclave have these kind of characteristics:

a. Inertness to acids, bases and oxidizing agents.

b. Leak-proof with unlimited capabilities to the required temperature and pressure.

c. Long-time duration, so that, no machining or treatment is needed after each experimental run.

In this research; PTFE (polytetrafluoroethylene)-lined acid digestion bombs were used as reaction autoclaves shown in Figure 2.1. These are provided from Parr Instrument Company (Illinois, USA) and removable Teflon is used as a lining material. Mostly, experiments are applied under mild hydrothermal conditions, in which the operating temperature is maximum 250 °C and maximum pressure is 1800 psi. Teflon is the most usable lining material for these kind of experiment because it has a larger coefficient of thermal expansion versus the material in which it is enclosed. During heating and cooling, the Teflon material expands. Thus, it is useful to apply a constant pressure on Teflon by a spring loaded closure (Byrappa and Yoshimura 2001).

In the hydrothermal synthesis with these autoclaves pressure changes on the nature of the solution, the degree of filling and the temperature. When the operating temperatures exceed the limits of the autoclave, the vapor pressure of the solution increases and the durability of materials that compose the autoclave decreases Moreover, the solutions tend to expand and fill a space 25% larger than its standard value. There must be sufficient vapor space in the autoclave. Thus liquid is not filled totally and increasing hydrostatic pressure will not destroy it.

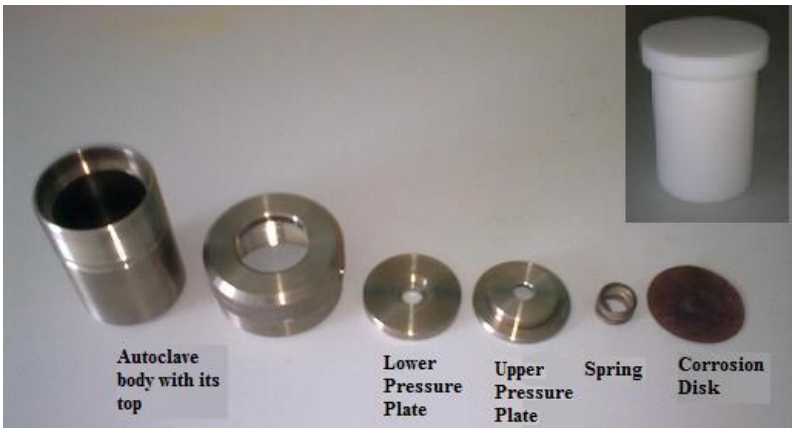

Figure 2.1. Schematic representation of an autoclave with its parts. (Inset shows the Teflon liner)

In this experiment, 23 mL Teflon lined reaction autoclaves (Parr Instruments – model 4749) are used during the hydrothermal treatment. After adding the precursor materials to the Teflon liner, it was placed in an autoclave covered first corrosion and rapture disks. Then, the spring with upper and lower pressure plates were placed. Finally, with a screw cup was firmly closed.

2.2. Characterization Techniques

Like synthesis and fabrication of cerium oxide nanoparticles, characterization part is also very important. It must be known, what the structure and composition is lack of microscopic techniques was a big handicap for first researhers that they could not measure and manipulate their materials. As microscopic techniques developed namaterial characterization has become more obvious to understand. X-ray diffraction (XRD) is the first characterization method for cerium oxide nanoparticles. Each crystalline has a unique X-ray powder pattern like finger prints. After proving the material is our desired product, structural characterization is required. Transmission Electron Microscopy (TEM) and Scanning Electron Microscopy (SEM) techniques is applied. Also to determine the optical properties of cerium oxide nanoparticles UV-VIS Spectrophotometer and Fluorescence Spectrosphotometer are used.

2.2.1. Structural Characterization

2.2.1.1. X-ray Diffraction

X-ray diffraction (XRD) which is a vigorous method can be used for investigation of crystal structure of a solid with lattice constants and geometry. On the other hand, it can be also used for orientation of single crystals, orientation of defects in crystal structure and identification of unknown solids (Cao 2004). X-ray region is identified with a wavelength of approximately 0.5-2.5Å in electromagnetic spectrum. X-ray diffraction with typical instrumentation can be seen in Figure 2.2. Under the high voltage system, high speed electron with a metal target collided to produce X-rays in X-ray tube. Beam of X-rays fall on a specimen as it generated, the crystalline phases in the specimen are diffracted according to the Bragg's law:

$$n\lambda = 2d\sin\theta \tag{2.1}$$

where n is the order of reflection, λ is the wavelegth of incident x-ray, d is the interplanar spacing between planes of a crystal and θ is the angle between incident beam and specimen surface (Cullity 1978).

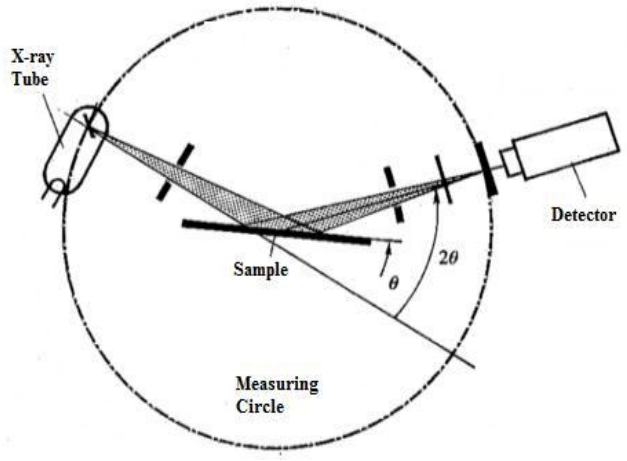

Figure 2.2. The X-ray Spectrometer
(Source: Smart and Moore 1996).

Diffracted X-ray intensity is measured kind of function of the diffraction angle, *2θ* and the specimen's orientation. This diffraction pattern is used to obtain information of the structural properties and to define the specimen's crystalline phases. It is a group of lines or peaks that has discrete intensity and position. These intensities are charactrestic feature of a material. Cerium oxide x-ray diffraction pattern can be seen in Figure 2.3.

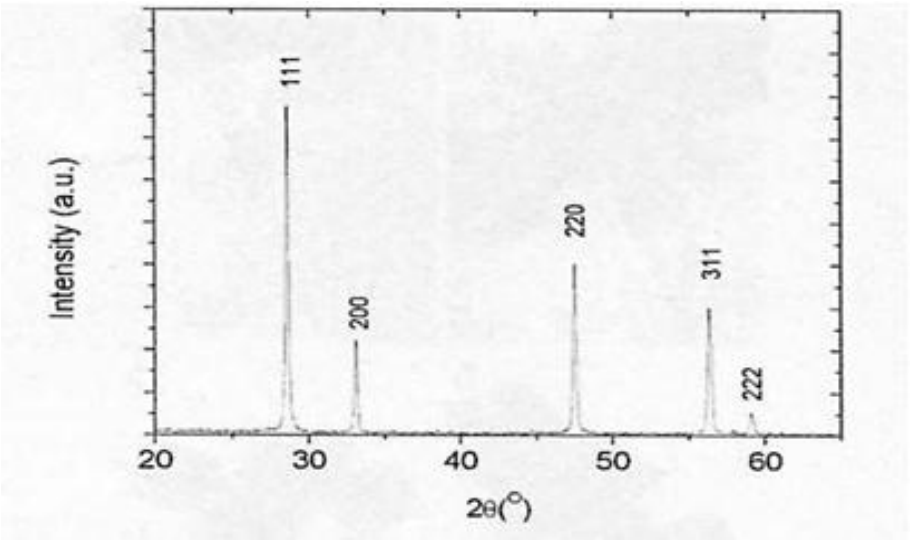

Figure 2.3. Typical XRD spectrum of cerium oxide nanoparticles (Source: Yang, et al. 2007).

When the diffraction pattern is acquired, then it is compared with the known published patterns. Whether a substance is a common type, it pairs one of the known patterns. Crystalline substances with standard patterns are expensed in the powder diffraction file, JCPDS (Joint Committee on Powder Diffraction Standards). This database includes more than 35000 entries and enhances every year. Whether powder diffraction pattern has never been aggregated before, some hypotheses can be made on structural type (Smart and Moore, 1996).

Mean of crystallite size (D) measurements can be done by using x-ray diffraction pattern with using Debye Scherrer's formula to the most intense peak:

$$D = \frac{0.9\lambda}{B\cos\theta_B} \qquad (2.2)$$

where λ is the wavelength of radiation, B is the full width at half maximum (FWHM) of the Bragg peak on the 2θ scale in radians and θ_B is the Bragg angle. Peak expanding appears because of the nano scale nature of crystal structure and this formula calculates peak expanding in the way of crystallite size. Nevertheless, it should be mentioned that Scherrer's formula can generate different results from the true particle sizes due to forming twinned nanostructures. Furthermore, X-ray diffraction uses only a small quantity of powder and it only assures the collective information of the particle sizes (Cao 2004).

In this study, X-ray powder diffraction (XRD) measurements were done by using Philips X-pert Pro Powder Diffractometer with CuKα radiation. (λ=1.5406 Å) Source of X-ray is the Philips high intensity ceramic sealed tube and data was collected for 2θ values of 20° to 70°.

2.2.1.2. Transmission Electron Microscopy (TEM)

A beam of electron is transmitted with a specimen to form an image in transmission electron microscopy (TEM). The "light source" emits electrons at the top of the microscope and these electrons travel along the vacuum in the column of the microscope. Electromagnetic lenses are applied to focus the electrons into a very thin and dense beam as the glass lenses focusing the light in the light microscopes.The electron beam then penetrates the sample studied. Some of the electrons can be scattered and dissappeared from the beam due to the density of the material present in the sample. Unscattered electrons strike a fluorescent screen, a layer of photographic or a CCD camera which allows to a "shadow image" of the sample with its discrete parts showed in diverse contrast according to their density (Wikipedia 2012).

A light microscope represents a magnification which is limited by the wavelength of light as a TEM instrument uses electrons as "source" and the much lower wavelength of electrons makes thousand times better resolution than a light microscope possible. TEM technique can define the objects in size of a few Angstroms (10^{-10} m). Materials in near atomic levels can be studied by new generation high resolution instruments. Thus TEM is an important tool in medical, physical, biological and materials studies (Nobel Web AB 2007). TEM is an expensive and destructive technique besides being one of the most advanced surface analysis techniques. Some of

the restrictions for materials are sensitivity to electron beam radiation, resulting in a loss of crystallinity and mass. Preparation of sample is another problem and it is a consultant issue.

2.2.1.3. Scanning Electron Microscopy (SEM)

In the early 1960s scanning electron microscope was invented. The principle of the microscope is scanning the surface of solid material with a beam of electrons. Energy range of electron beam is between few hundred eV to 100 keV. One or more condenser lenses focused the beam in to a spot sized 0.4nm to 5nm. Electron beam is deflected vertically and horiontally that provides scanning over a rectangular area of the sample surface.

When the electron beams contact with the surface of the sample backscattered, secondary and Auger electrons are produced. In order to study the surface backscattered and secondary electrons should be taken in to consideration (Skoog, et al. 1998, Strobel and Heineman 1989). Secondary electrons emit the surface electrons on the other hand backscattered electrons are reflected source electrons. These emitted and reflected electrons are detected in photomultiplier tube and 2D or 3D image is illustrated on the monitor. The schematic of Scanning Electron Microscopy is illustrated in Figure 2.4.

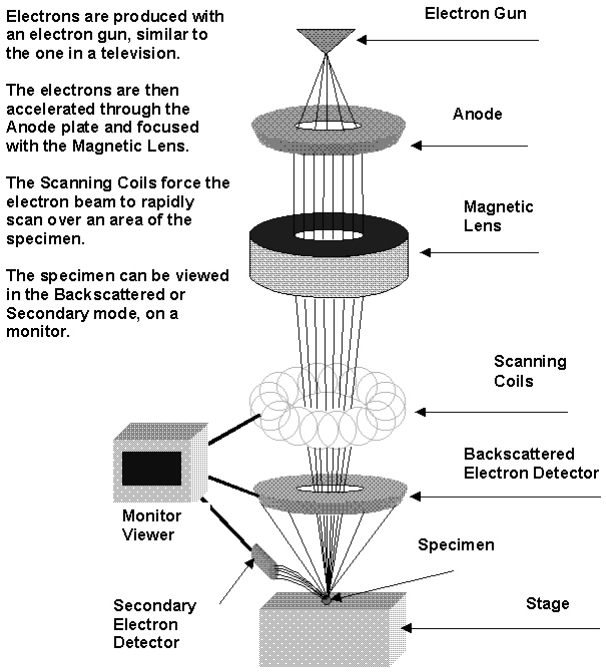

Figure 2.4. Schematic of Scanning Electron Microscopy
(Source: Renssealer Polytechnic Institute 2007)

In this study Philips XL-30S FEG model instrument was used. The powder samples were attached on to carbon tapes supported on metallic disks. With the different magnifications, sample surfaces were scattered and the images were illustrated. Also EDS analysis were applied simultaneously at selected areas of solid surface in order to observe which elements are exist.

2.2.1.4. UV/VIS Spectrometry

Basically, UV/VIS absorption spectroscopy measures the energy of the light after the beam of light reflects from sample surface or passes through the sample. UV/VIS light has enough energy to excite outer electrons to higher energy levels. The handicap of UV/VIS spectra is, it is not an ideal method for sample identification. On the other hand, it is very useful for quantitative measurements. Beer-Lambert Law is applied in order to determine the concentration of an analyte in solution. Commercial UV/VIS spectrophotometers define the working spectral range as approximately 190 to 750nm. Since the human visual acuity range is approximately 400 to 750 nm, UV/VIS is very appropriate for charaterizing the absorption and transmission. To characterize the

optical or electronic properties of materials, at least a portion of the UV/VIS spectrum is required. For UV/VIS measurements the light source is usually deterium discharge lamp, for visible and NIR measurements tungsten-halogen lamp is used as the source. Holographic graring in single or double monochromator or spectrograph deispers wavelengths of the light sources and then the monochromator slit width or array-element width determines the spectral bandpass. Stray light limits the quantitativeabsorbance measurements. In order to prevent this problem , spectrometer designs and optical components are optimized to reject the stray light. As the detector in single-detector instruments, photodiode, phototube or photomultiplier tube is used (Skoog, et al. 1998)

2.2.1.5. Fluorescence Spectroscopy

A material which gains energy from a light source, absorbs photons at some wavelength and elevates electron's energy from ground state to higher levels. This duration can be defined as transition from ground state to promoted state of an atom or transition from valance band to the conduction band at a semiconductor crystal or polymer. Then the system induces a relaxation which means promoted electrons will return to the ground state, after a characteristic lifetime in promoted state. All this process is called fluorescence. In fluorescence, the wavelength of the emitted light is long in comparison with the incident light (Cao 2004). The emission spectrum can be described as a plot of of emission against wavelength for any given excitation wavelength. Rare earth ions which have typical line spectra depend on intra-4f transitions. Fluorescence spectra is relevant to 4f-5d transitions and they are containing broad spectral line width which are crystal field relevant and can be detected by the size and structure of crystal (Yan and Yan, 2008). Cerium oxide nanoparticles show strong emission peak around 400 nm. and their spectrum includes particle size dependent shifts. It can be investigated that the morphology depend on feature, size and defect level effect the fluorescence spectrum of cerium oxide nanoparticles. Varian Cary 50 UV/VIS and Varian Cary Eclipse Fluorescence Spectrometer under excitation at 290 nm. at room temperature were used for determining optical properties.

2.2.1.6. Gas Chromotography (GC)

A gas chromatograph (GC) is an analytical instrument that measures the content of various components in a sample. The analysis performed by a gas chromatography is called gas chromotography.

Principle of gas chromatography: The sample solution injected into the instrument enters a gas stream which transports the sample into a separation tube known as the "column". Helium or nitrogen is used as the so-called carrier gas. The various components are separated inside the column. The detector measures the quantity of the components that exit the column. To measure a sample with an unknown concentration, a standard sample with known concentration is injected into the instrument. The standard sample peak retention time and area are compared to the test sample to calculate the concentration (Shimadzu 2012). Agilent 6890N instrument was used in this study.

2.2.1.7. Gas Chromotography-Mass Spectroscopy (GC-MS)

Gas chromatography (GC) is a method used to help identify a mixture of compounds by separating compounds according to each compound's retention time. Compounds with a lower molecular weight will elute out earlier than compounds with higher molecular weights due to differences in boiling points. Smaller structures have lower boiling points and will thus elute faster than those with higher boiling points. It then follows that the compounds with the lower boiling points will have shorter retention times. Another advantage of GC is that it can be used to determine the purity of compounds. By looking for additional peaks in a sample that are not present in the pure compound, one can gain knowledge about purity. Peak areas of additional peaks can provide an indication of the degree of contamination (Skoog, et al. 2008). Factors other than the boiling points of compounds will also affect separation. Other factors that determine the separation are: the polarity and physical size of the molecules, the column type, and the number of theoretical plates. The polarity of compounds should be considered because polar compounds will have a longer elution time on a polar column while a nonpolar compound will elute in shorter times (Skoog, et al. 2008).

The mobile phase flow rate also affects the appearance of peaks on the chromatogram (Skoog, et al. 2008). If the flow is too fast, peaks may not separate out as well, however, if the flow is too slow, band broadening may occur. Column efficiency is another aspect that must be taken into account. The smaller the height equivalent to a theoretical plate the more efficient the column (Skoog, et al. 2008). In the actual process of running a gas chromatograph, a sample is run by using a syringe to inject your compound into the injector port, which leads to a column. A carrier gas is utilized in order to carry the sample on to the column. The various compounds in the sample will separate and result in the appearance of peaks at different locations on your chromatogram (Zubrick 1988). Compounds are identified through their chemical compositions which can be obtained by a variety of means. Mass spectroscopy is one of the chemist's tools in their arsenal. Through mass spectroscopy, one can determine the molecular weight, molecular formula, and the functional groups present on a compound (Skoog, et al. 2008). The molecular weight can be determined by identifying the molecular ion peak. Looking at the mass to charge ratio (m/z) and the distribution of isotopes, one is able to determine an average mass for a compound. The molecular formula for a compound can then be ascertained from the relative peak heights of the isotopes. When looking at mass spectra, the majority of peaks that appear are attributed to fragments; these fragments are pieces of the original compound that have separated from the compound. The appearance of these fragments makes interpretation slightly more difficult, which is why the use of a library can become advantageous. By comparing your sample to knowns, a positive identification is possible. The main advantage of interfacing a gas chromatograph with a mass spectrometer is its efficiency. With combined instrumentation, only one sample needs to be prepared. This saves on both time and materials. The physical bench space taken up is minimized as well. The GC/MS/MS allows one to obtain more detailed information about unknown compounds faster and more easily than the instruments separately. Combining these technologies allows one to analyze more complex compounds faster than a GC, MS, or GC/MS (Skoog, et al. 2008).

2.2.1.8 Nuclear Magnetic Resonance (NMR)

There are two main types of nuclear magnetic resonance (NMR) technology that you will typically encounter in your career as an undergraduate: proton NMR (^{1}HNMR) and carbon NMR (^{13}CNMR). A ^{1}HNMR works by looking at the change in energy between the two energy states of protons. These states are affected by the magnetic field, which is dependent on the electrons around the protons, through the bonds and corresponding atoms. Chemists can identify a compound by looking at the chemical shifts produced. Chemical shifts result from the "small magnetic fields that are generated by electrons as they circulate around nuclei" (Skoog, et al. 2008). This is essentially the area on a graph where a peak occurs; these peaks are indicative of various proton interactions within the molecule. By looking at the height of the peak, one is able to tell the number and types of protons, which subsequently helps identify a particular compound. Examination of charts and tables correlating chemical shifts to specific functional groups further aids in analyzing NMR spectra (Skoog, et al. 2008). Combining all of the aforementioned information enables one to determine a structure for a compound. The identity of the compound can then be confirmed by comparison to a known reference.

A proton is among the easiest nuclei to study due to its abundance. Due to the spin of this positively charged proton, a magnetic moment is created. We can use NMR technology to determine the spin of protons. When the proton is exposed to a magnetic field it will orient itself in such a way as to align with or against the magnetic field. Life, however, is not so simple when looking at complex molecules and not just protons. Due to electrons in molecules, the nucleus will be shielded; the electrons will inhibit the nucleus from feeling the full effects of the magnet (Wade 2009). Thus shielding should decrease with increasing electronegativity of adjacent groups since the more electronegative groups will withdraw the electrons from adjacent protons, leaving the nucleus more exposed to the effects of the magnetic field (Skoog, et al 2008). This is where NMR becomes useful. By looking at shielding, we are able to approximate a structure for a compound. Carbon NMR is similar to that of proton NMR, but instead looks at the "magnetic environments of the carbon atoms themselves" (Wade 2009). Since the ^{13}C isotope is relatively rare, ^{13}C NMR is significantly less sensitive than ^{1}H NMR (Wade 2009). While the decreased sensitivity is a disadvantage for carbon NMR,

an advantage is that it gives us information concerning the backbone of a compound instead of the branches (Skoog, et al. 2008). Something that often gets confusing is the idea of lower and higher fields. Protons that are less shielded will appear more downfield. Another sometimes troubling issue is spin-spin splitting. This is when chemical shift peaks split due to the interaction of one nucleus's magnetic moment with the magnetic moments of immediately adjacent nuclei (Skoog, et al 2008). Varian 400-MR (400 MHz) was used to monitore the results of the reactions in this study.

2.3. Experimantal Procedure

2.3.1. Synthesis of Cerium Oxide Nanoparticles

In this study 0.5 g $Ce(NO_3)_3.6H_2O$ was dissolved in 3 mL of pure water and then 15 mL of CsOH and RbOH solution was added gently. Then the solution mixture was stirred about 30 minutes and transferred in to 23 mL autoclaves and hydrothermal synthesis technique applied for different reaction times and temperatures. Finally the the product centrifugated at 6000 rpm and dried at aboout 60 °C to 70 °C for further processes (Yang, et al. 2007). Then nanoparticles were characterized by XRD, SEM, TEM, UV-VIS Spectrophotometer and Fluorescence Spectrophotometer.

2.3.2. General Methods for Catalytic Transformations of Chalcones

2'-Hydroxychalcone was commercial grade and used as supplied. Reactions were monitored by thin layer chromatography by using Merck TLC plates (Silica gel 60 F254). Chromatographic separations and isolations of compounds were performed by column chromatography. 70-230 mesh silica gel was used for column chromatography. Solvents were also commercial grade and were used as supplied. The synthesized products were analyzed by GC using Hydodex-beta-3P column (25 m, 0.25 mm ID, FID detector temperature: 320 ^oC, inlet temperature: 300 ^oC, temperature programming: 40 ^oC, 5 ^oC/min, 300 ^oC (5min.), flow rate: 1.5 mL/min), GC-MS (HP 5MS, 25 m, 0.25 mm ID, inlet temperature: 300 ^oC, temperature programming: 40 ^oC, 5 ^oC/min, 300 ^oC (5min.), flow rate: 1.5 mL/min) and ^1H NMR data was recorded on Varian 400-MR

(400 MHz) spectrometer. Chemical shifts for ^{1}H NMR is reported in δ (ppm). $CDCl_3$ peaks were used as reference in ^{1}H NMR (7.26 ppm).

2.3.3. Synthesis of Flavone (3)

A mixture of 30.0 mg 2'-hydroxychalcone **(1)** and 110 mg sodium acetate (or instead 30 mg of NaOH treated ceria nanoparticles synthesized in presence of 0.1M RbOH for 24 h. and 240 ^{o}C) in anhydrous DMSO (DMF or ethanol) was prepared and stirred for 24 h. at 100 ^{o}C in presence of DMSO and DMF, (in presence of ethanol). Resulting solution was extracted with ethyl acetate (3x15 mL) and pure water (3x15 mL). Resulting organic phase was dried over $MgSO_4$. After the removal of the solvent under vacuum, crude product was purified by column chromotography on silica gel (1:12 EtOAc/Hexanes) to furnish flavone **(3)**. Rf=0.5 (ethyl acetate/hexane, 1:4). Yields of the reactions are given in Table 3.4.

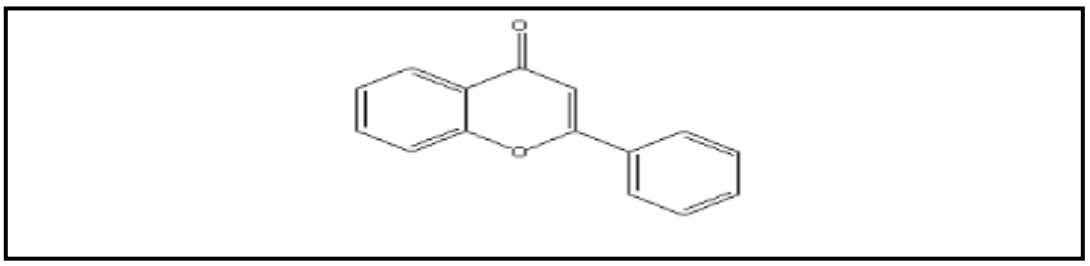

Figure 2.5. Flavone **(3)**

GC-MS (EI, m/z): 222 (100, M^+), 223 (15), 194 (48), 165 (15), 120 (56), 92 (30), 63 (11); GC, Rt=21.9; ^{1}H NMR (400 MHz, $CDCl_3$) δ ppm 6.85 (s, 1H), 7.40 - 7.48 (m, 1H), 7.51 - 7.62 (m, 4H), 7.67 - 7.76 (m, 1H), 7.92 - 7.99 (m, 2H), 8.26 (dd, *J*=8.20, 1.60 Hz, 1H)

2.3.4. Synthesis of Unsubstituted Chalcone

A mixture of 15 ml 15% NaOH solution, 7.5 mL ethanol and 3ml acetophenon was heated and stirred for 30 min. in the 70 ^{o}C water bath. While stirring, 2.5 mL of benzaldhyde was added gently in to the mixture. After stirring, the mixture was cooled

to 0 ^{o}C in an ice bath then the product was collected and filtrated. Finally crude product was purified by column chromotography on silica gel (1:12 EtOAc/Hexanes) Rf=0.7 (ethyl acetate/hexane, 1:4)

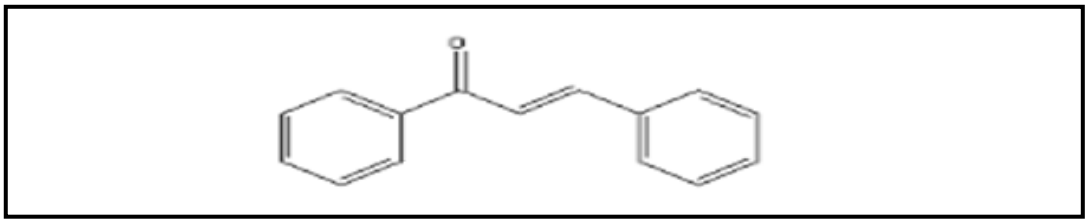

Figure 2.6. Unsubstituted chalcone **(4)**

^{1}H NMR (400 MHz, $CDCl_3$) δ ppm 7.40 - 7.45 (m, 3H), 7.48 - 7.56 (m, 3H), 7.56 - 7.62 (m, 1H), 7.62 - 7.68 (m, 2H), 7.82 (d, *J*=15.65 Hz, 1H), 7.99 - 8.06 (m, 2H); GC, Rt=19.6; GC-MS (EI, m/z): 77 (100, M^{+}), 207 (75), 208 (65), 51 (31), 103 (46), 131 (38), 178 (9), 179 (16), 209 (8).

CHAPTER 3

RESULTS AND DISCUSSION

3.1. Morphological and Structural Characterization

Unique XRD pattern of cerium oxide nanoparticles is shown in Figure 3.1. Different alkali bases CsOH and RbOH are used in order to synthesize nanoparticles. XRD pattern is the proof of the characrteristics of CeO_2 and all the reflections are indexed to cubic fluorite structure (JCPDS – 81-0792) with a lattice parameter of 5.412 Å. Unique XRD pattern shows whether Ce^{3+} defect states exists or not in CeO_2 nanoparticles. Both Ce^{4+} and Ce^{3+} valance cations exist in bulk structure and as cerium oxide is reduced from 4+ to 3+ lattice constant increase, electrostatic forces between particles decrease (Tsunekawa, et al. 2000).

Oxygen vacancies and oxygen spacing control are used in many applications of cerium oxide nanoparticles. Oxygen storage capacity controls many processes such as migration and formation of oxygen vacancies. Particles, having smaller size has larger surface areas which means having high oxygen storage capacity.

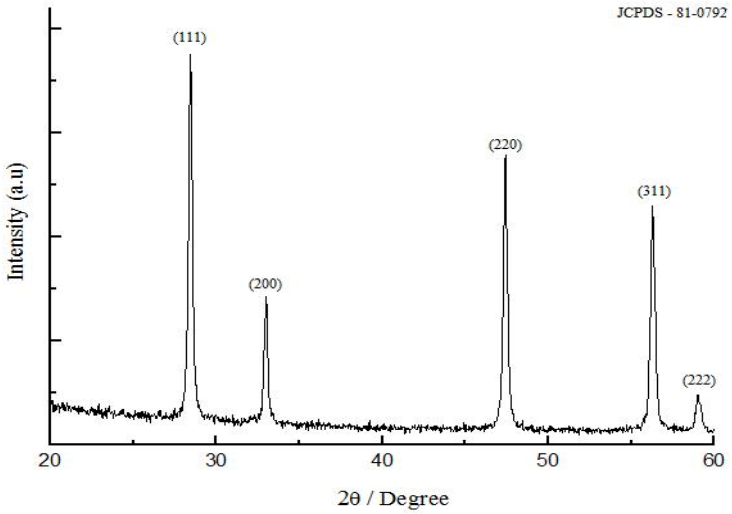

Figure 3.1. XRD pattern of as-prepared CeO_2 nanoparticles.

Cubic and rod like shape of cerium oxide nanoparticles are investigated with scanning electron microscope. EDX spectrum shows the presence of Ce and O atoms in particle Figure 3.2. shows the EDX spectrum and SEM images of cerium oxide nanoparticles.

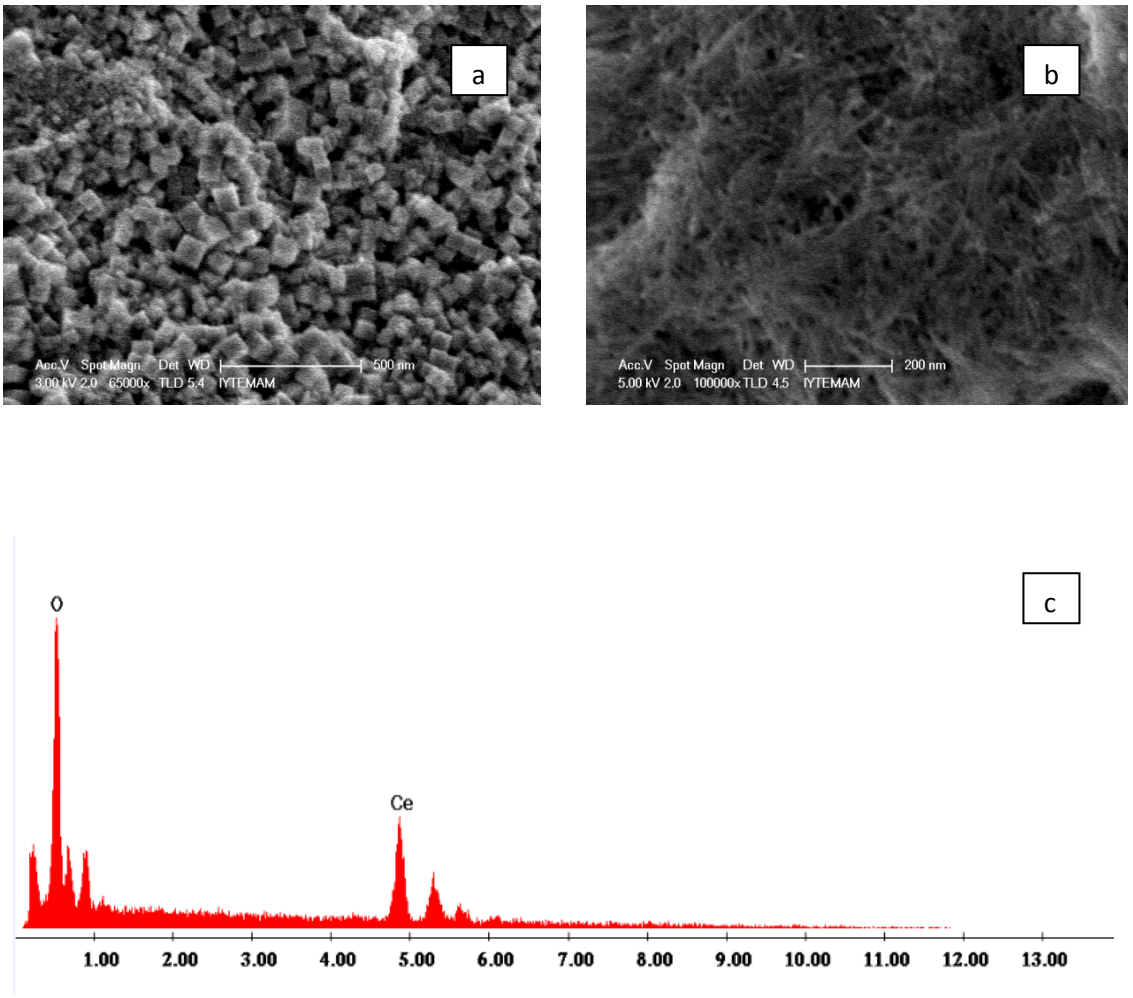

Figure 3.2. (a) and (b) SEM images, (c) EDX spectrum of CeO_2 nanoparticles.

TEM images in Figure 3.3. show single CeO_2 cube synthesized with CsOH and RbOH alkali base and it is composed of well crystallized nanosized grains with the clear view of lattice fringes.

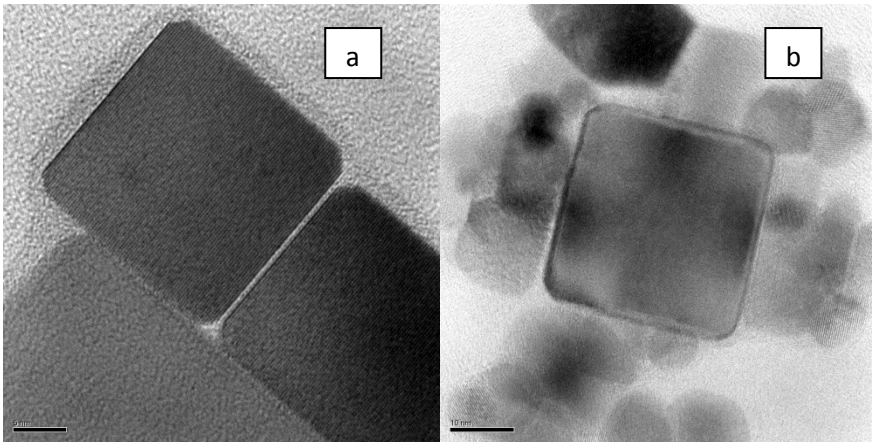

Figure 3.3. HRTEM image of a single CeO_2 nanocube synthesized at 240 °C for 24 h. in presence of (a) CsOH (b) RbOH.

3.2. Controlling Factors on Size and Shape of CeO_2 Nanoparticles

This study proove that alkali type, concentration, reaction type and reaction temperature effects size and shape of nanoparticles.

3.2.1. Effects of Alkali Base Type and Concentration

First of all CsOH was used by changing the concentration and keeping the reaction temperature and time constant. As the concentration increases both morphology and size of nanoparticles changes. Particle size of cubic structured nanoparticles become larger when the concentration increase and high monomer concentration result in branched structures like cubic shape (Peng 2003). Figure 3.4 shows that phenomena.

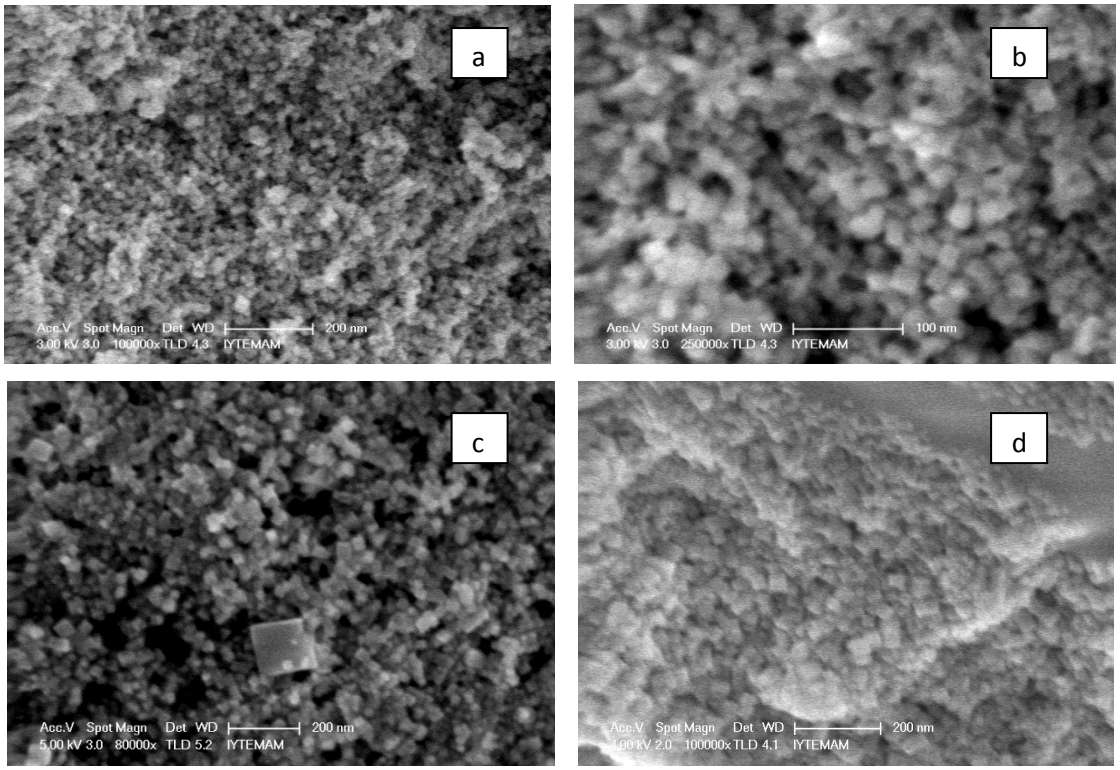

Figure 3.4. SEM images of obtained CeO_2 nanoparticles. Precipitated at 240°C for 24 h. Used base was (a) 0.1 M CsOH, (b) 0.5 M CsOH, (c) 1M CsOH and (d) 8M CsOH.

Variation of concentration of RbOH also shown. As in Figure 3.5 concentration dependence of particle size was observed.

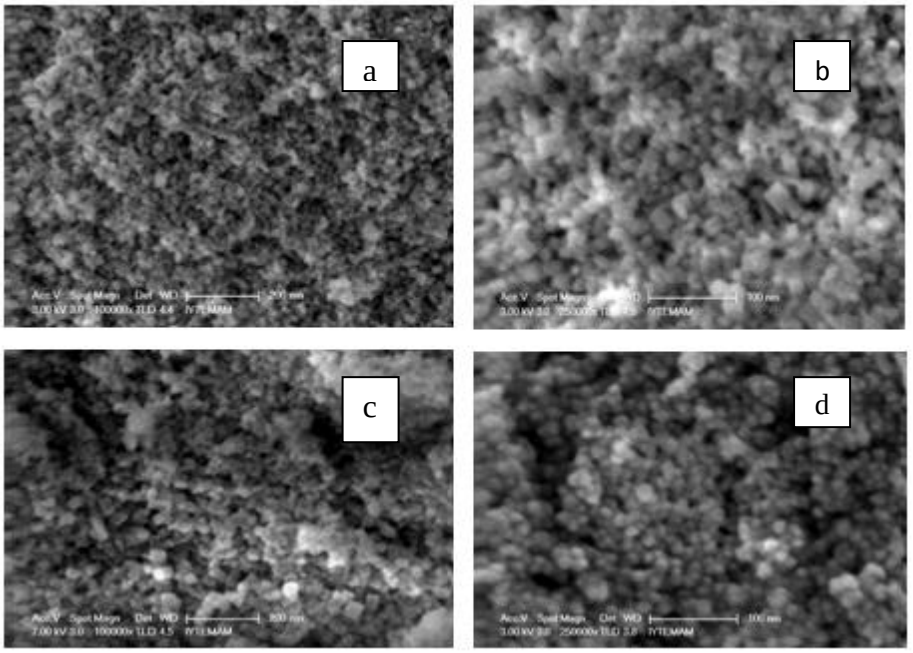

Figure 3.5. SEM images of obtained CeO_2 nanoparticles. Precipitated at 240°C for 24 h. Used base was (a) 0.1 M RbOH, (b) 0.5 M RbOH, (c) 1M RbOH and (d) 8M RbOH.

XRD patterns in Figure 3.6 for RbOH showed that as the concentration was increased, peaks of CeO_2 became intense and sharper. Generally, wider the XRD peak, lower the crystallite size of nanoparticles (Lian, et al. 2004).

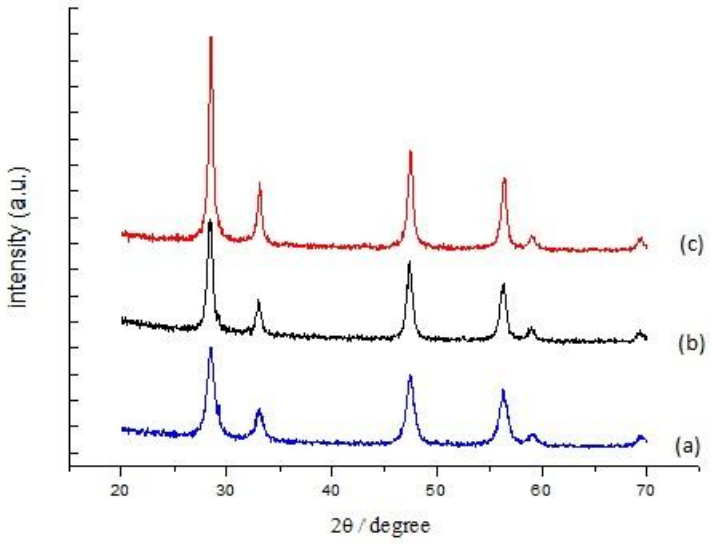

Figure 3.6. X-ray diffraction patterns of CeO_2 nanoparticles prepared at 240°C for 24 h. (a) 0.1M RbOH, (b) 1M RbOH and (c) 8M RbOH.

XRD patterns for 8M CsOH and 8M RbOH bases under same conditions (reaction temperature, reaction time) are shown in Figure 3.7. XRD peaks become sharper and more intense for RbOH that indicates nanoparticles in presence of 8M RbOH have larger crystalite size than that of 8M CsOH.

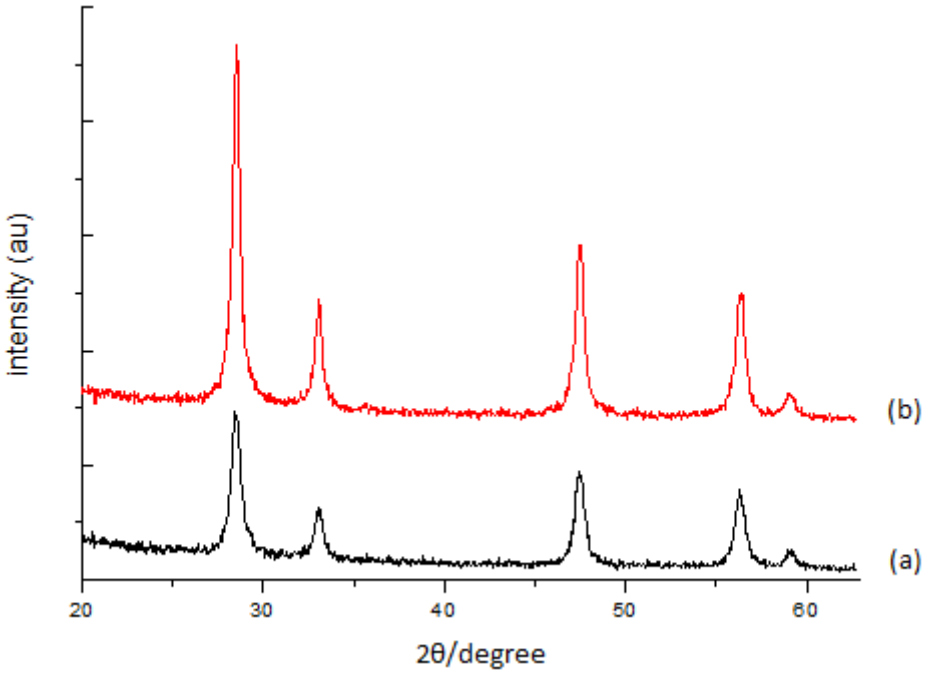

Figure 3.7. XRD patterns of the precipitated powders obtained from aqueous solutions containing CeO_2.The heating temperature was 240 °C for 24 h. The used base was (a) 8M CsOH, (b) 8M RbOH.

From the most intense peak crystallite sizes were determined by applying full width at half maximum using Debye Scherrer equation. Average crystalite size is directly proportional with the base concentration. As a result cerium oxide nanoparticles, synthesized at higher concentrations of RbOH and CsOH have larger average crystalite sizes than that of lower concentrations. As the concentration of alkali base increase and going from Cs to Rb, nanoparticles increase in size. Average crystallite size results are shown in Table 3.1.

Table 3.1. Average crystalite sizes calculated from the most intense (111) XRD peak as a function of alkali base type and concentration.

Temperature: 240 ^{o}C	Starting Bases	
Concentrations (M)	RbOH (nm)	CsOH (nm)
0.1	11	12
1	15	15
8	19	19

Particle size distribution was determined by measuring over 100 particle size from SEM and shown in Figure 3.8. Average particle sizes were varied with alkali base change. Experiments in presence of 8M CsOH alkali base provided average 24 nm and 8M RbOH alkali base provided average 35 nm particle size. These particle sizes are not consistent with crystallite sizes as they are completely different. Analysis of profile parameters in X-ray patterns is used to determine the crystallite size. When XRD measures the crystallite size, it probably detects the single crystal within the particle. Size analysis with profile widths gives the crystallite size. Domains that are separated by domain walls may exist within the particles. These domains cannot be detected with TEM or SEM. They only detect the particle sizes. Particle size measurement is done to the whole powder after crystal growth and it can contain more than one crystal. Therefore, it is logical to have larger particle size than crystallite size.

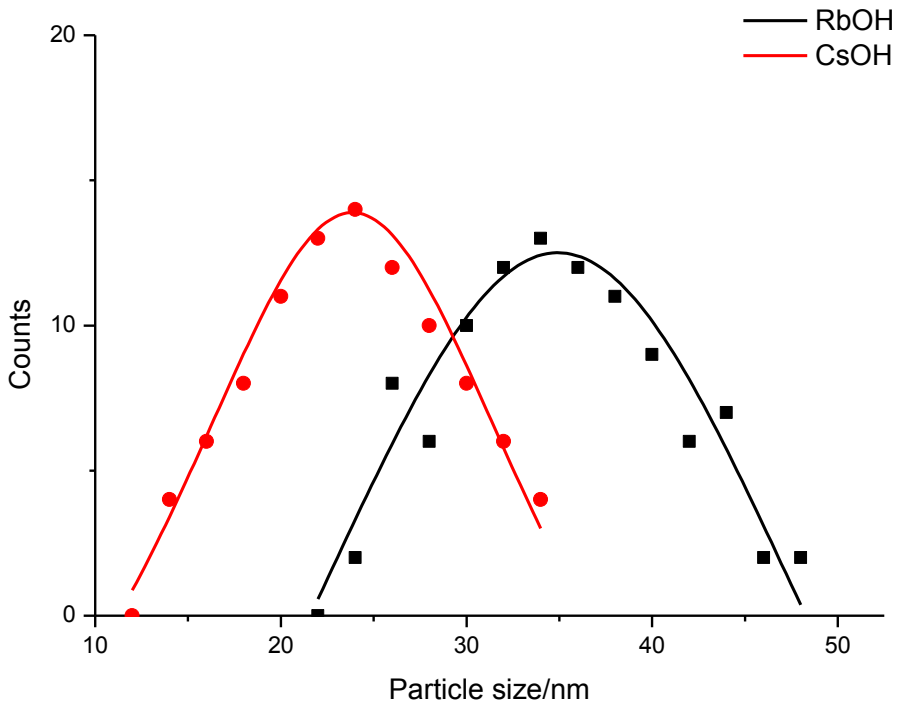

Figure 3.8. Particle size distributions of CeO_2 nanoparticles synthesized with RbOH and CsOH respectively.

3.2.2. Effect of Reaction Time

In this part of the study reaction times has changed in order to understand the formation process of cerium oxide nanoparticles at different reaction times. Nanoparticles were synthesized with 8M CsOH and 8M RbOH alkali base for the time intervals 1h, 12h, 24h respectively. The series of SEM images in Figure 3.9 and 3.10. show that 24 hours reaction time was the best choice for fabrication of CeO_2 nanoparticles. As the reaction time was increased nanoparticles favors from aggregated species to the cubic shapes. With the extension of time, CeO_2 nanoparticles may complete their nucleation and the growth of nanoparticles was based on the Ostwald ripening process that makes the crystallinity improved and the diameter grew. So, the aggragates recrystallize into single-crystalline nanocubes.

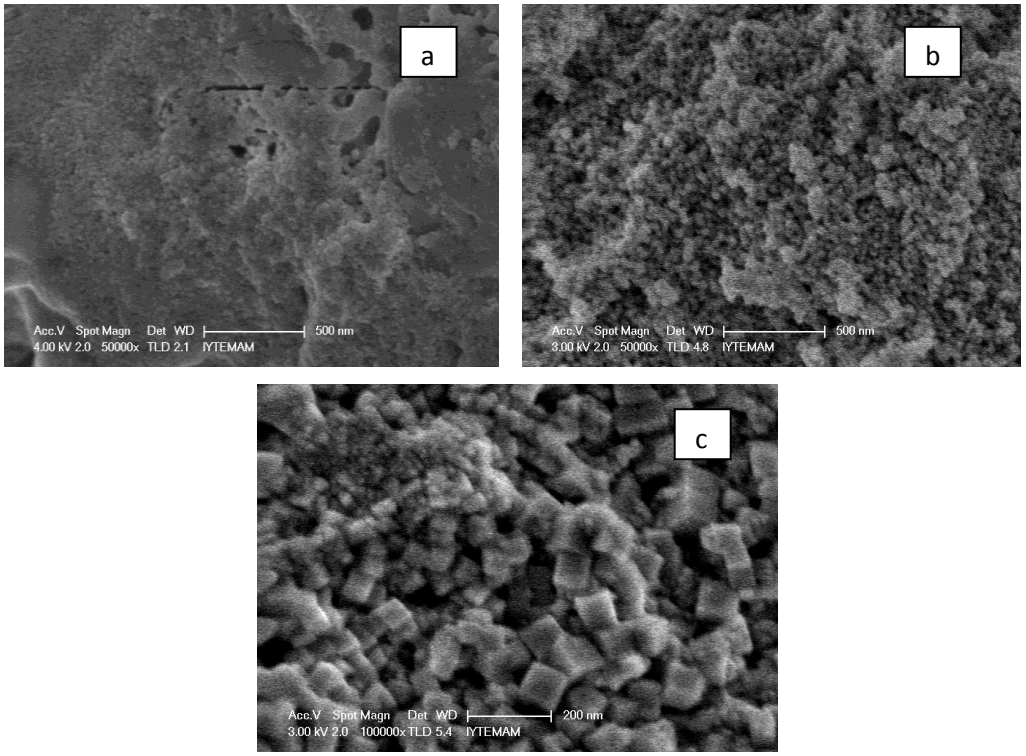

Figure 3.9. Series SEM images of morphology evolution of cubic CeO_2 nanoparticles with the stepwise prolonged reaction time (a) 1 h. (b) 12 h. (c) 24 h. RbOH was used as the base.

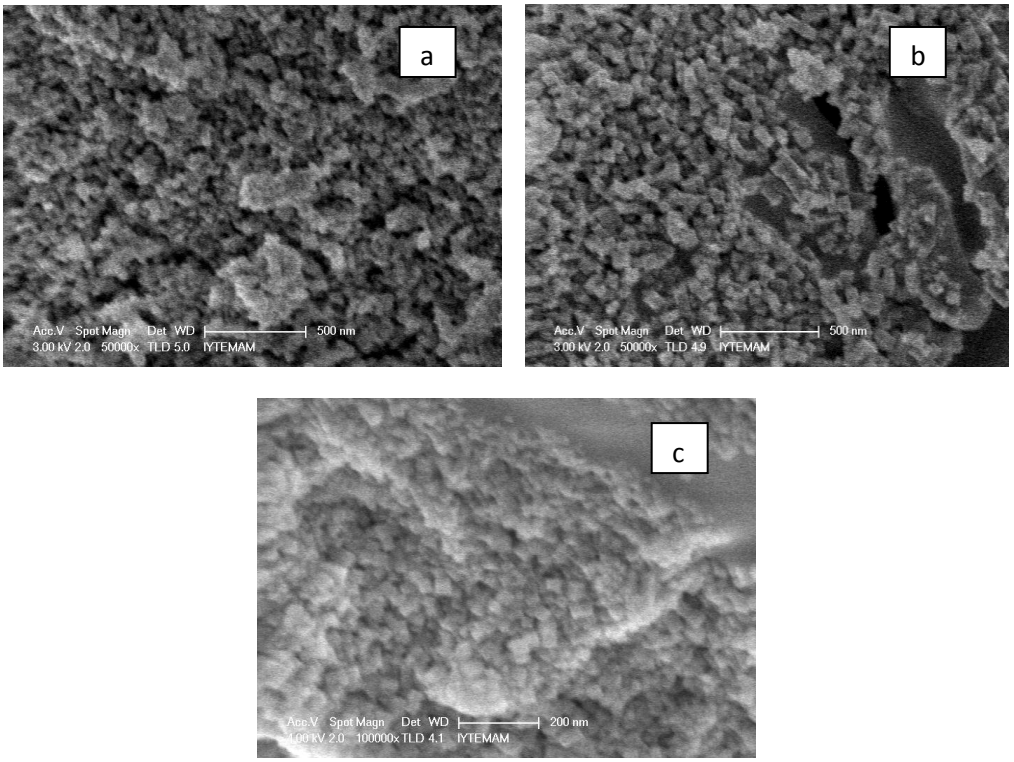

Figure 3.10. Series SEM images of morphology evolution of cubic CeO_2 nanoparticles with the stepwise prolonged reaction time (a) 1 h. (b) 12 h. (c) 24 h. used base was CsOH.

From the XRD patterns for RbOH illustrated in Figure 3.11, average crystallite sizes were determined by applying full width at half maximum to the most intense peak (111). Like alkali base concentration, reaction time is also directly proportional with the average crystalite size. Cerium oxide nanoparticles, synthesized at higher reaction times have larger average crystalite size than that of lower times The size calculation results are shown in Table 3.2.

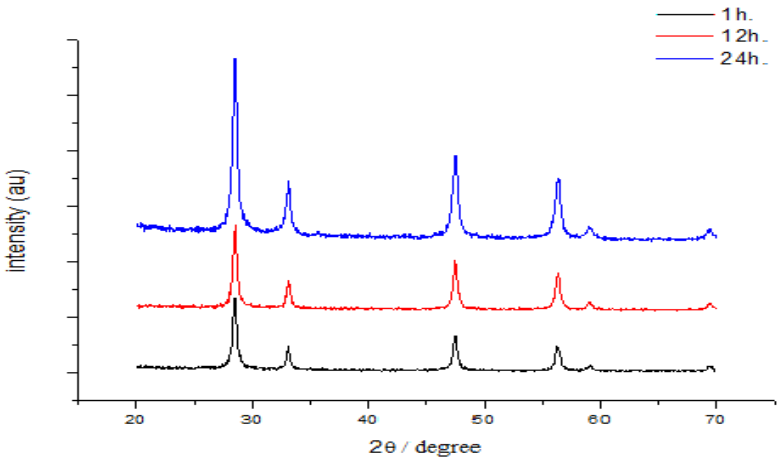

Figure 3.11. XRD pattern of CeO_2 nanoparticles in presence of 8 M RbOH for different reaction time intervals.

Table 3.2. Average crystallite sizes calculated from the most intense (111) XRD peak as a function of reaction time.

Temperature; 240 °C	Average crystallite size (nm)	
Reaction Time (h)	CsOH	RbOH
1	16	15
12	17	16
24	19	19

Furthermore, particle growth kinetics study was done in order to fully understand the evolution of nanoparticles against reaction time. Growth kinetics affects the electronic and mechanical properties of nanomaterials especially doped with other materials. They allow investigating the diffusion mechanisms of both pure ceria and doped ceria. Particle size distributions that are shown in Figure 3.12. and Figure 3.13. were determined by measuring over 100 particle sizes from SEM images. When the reaction time was increased, it caused particle sizes to increase. Then, the grain-growth depended on time analysed with the following equation:

$$D^n - D_o^n = Kt \tag{3.1}$$

$$K = K_o \exp\left(\frac{-Q}{RT}\right) \tag{3.2}$$

Where D^n is the is the grain size at time, t, D^n_o is the average grain size at time, t=0, n is the grain exponent, K is the rate constant, K_o is the preexponential constant, Q is the activation energy of grain growth, R and T are the gas constant and absolute temperature. For thermally activated processes ($D>D_o$), these equation can be simplified as;

$$D^n = K_o \exp\left(\frac{-Q}{RT}\right)t \tag{3.3}$$

In a constant temperature range, Q is a constant. Thus, grain exponent (n) can be found from slope of the plot of lnD vs. lnt which is illustrated in Figure 3.14. Particle growth rates were shown on Table 3.4. Based on this, cerium oxide nanoparticles synthesized with CsOH gave smaller particle growth rate than RbOH.

Table 3.3. Particle growth rates of CeO_2 nanoparticles in presence of different alkali bases.

Alkali Base	Particle Growth Rate (n value)
CsOH	2.39
RbOH	1.89

Chen and Chen (1996) found pure CeO_2 grain growth, obtained with homogeneous precipitation method, as 2, Zhang, et al. (2002) found the grain growth of nanoparticles, prepared by conventional mixed oxide method, as 3. We found somewhat close to their results. According to particle growth rate results of Kepenekçi, et al. (2011) CeO_2 nanoparticles' growth rate, synthesized with CsOH and RbOH is smaller than that of synthesized with NaOH, LiOH, and KOH. The reason is may be our synthesized materials have lower reactivity (Zhang, et al. 2003).

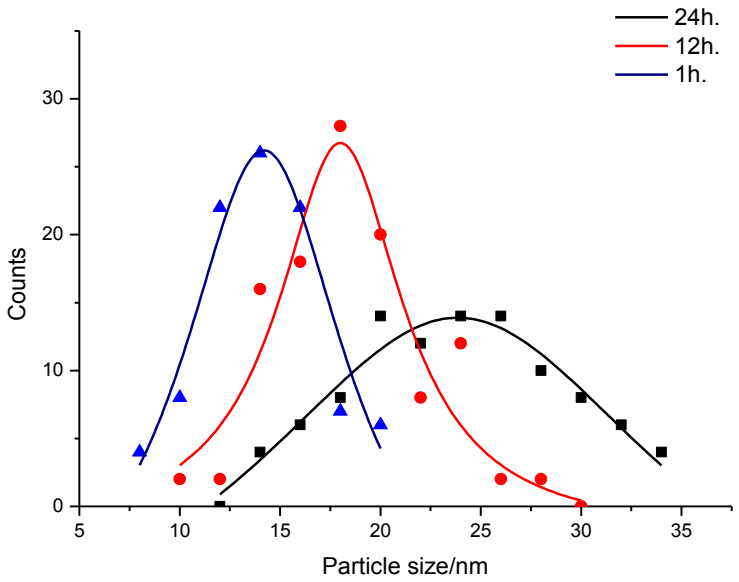

Figure 3.12. Particle size distribution of CeO_2 nanoparticles in presence of CsOH alkali base under different reaction times.

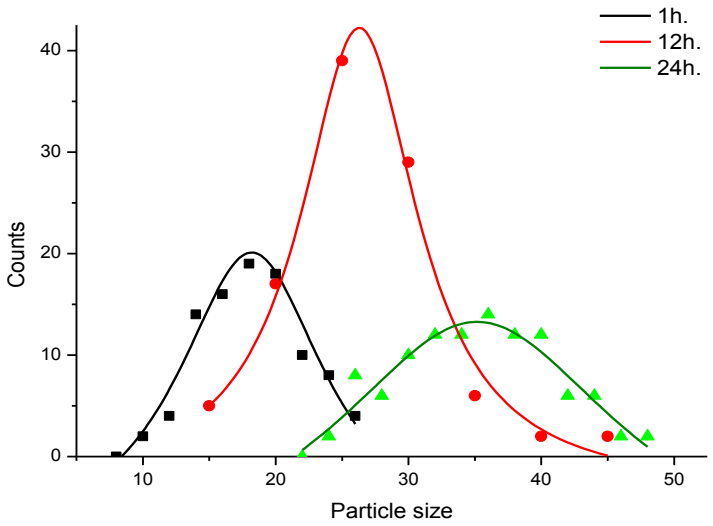

Figure 3.13. Particle size distribution of CeO_2 nanoparticles in presence of RbOH alkali base under different reaction times.

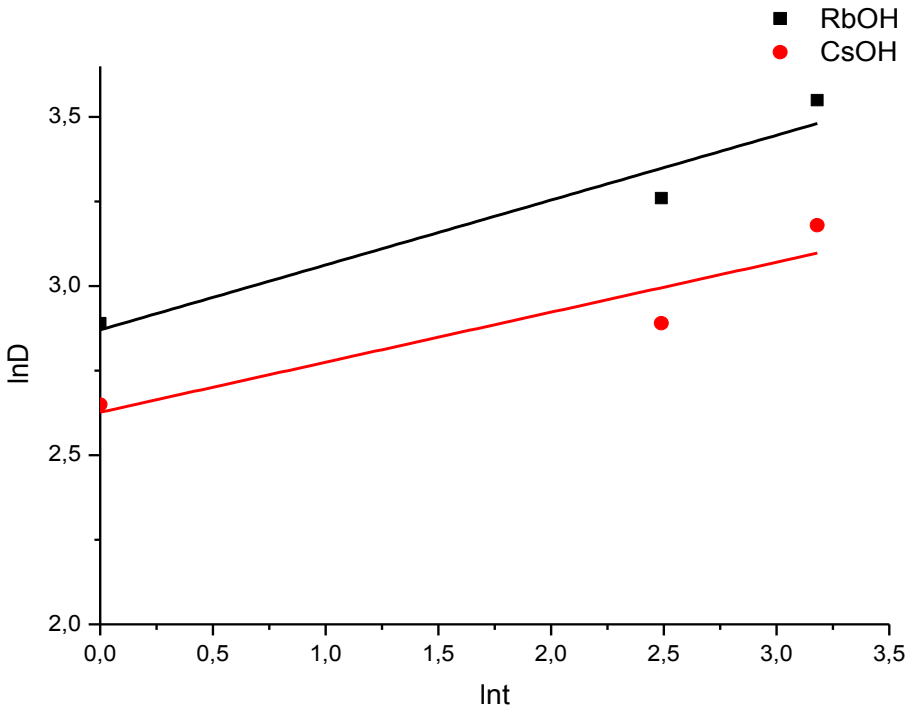

Figure 3.14. Plot of lnD vs. lnt for different alkali bases. The values of n were calculated from the slope of the best fit lines.

3.2.3. Effect of Reaction Temperature

Crystallite size and particle morphology were determined by fixing reaction time and changing hydrothermal reaction temperature. We observed rod-shaped nanoparticles at 120 °C as reported in literature (Yang, et al. 2007). When we increase reaction temperature to 240 °C cerium oxide naoparticles transforms in to cubic shape. Increasing temperature accelerates crystal growth as it is illustrated in Figure 3.15. and Figure 3.16. for both 8M RbOH and 8M CsOH.

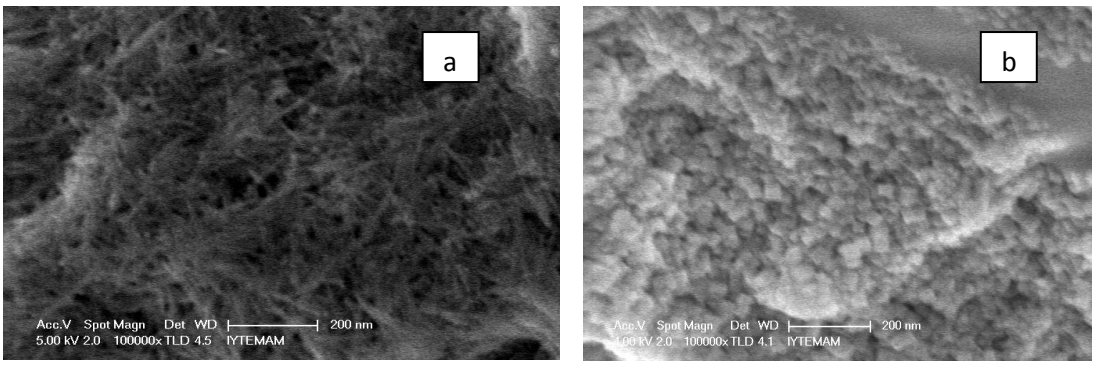

Figure 3.15. SEM images of obtained cubic CeO_2 nanoparticles. The used base was CsOH and the heating temperature was (a) 120 °C, (b) 240 °C for 24 h.

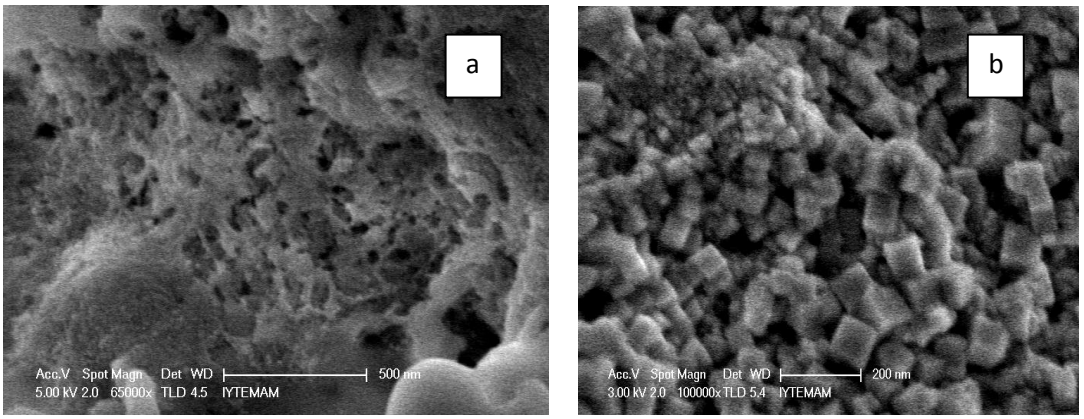

Figure 3.16. SEM images of obtained cubic CeO_2 nanoparticles. The used base was RbOH and the heating temperature was (a) 120 °C, (b) 240 °C for 24 h.

XRD studies prooves that increase in temperature promotes the formation of CeO_2 nanoparticles. The precipitated crystalline Ce_2O_3 ceria dissolves in water when the temperature is increased. At nucleation step concentration of ceria monomers increases and theyrecrystallize into nuclei and transform to various shapes. At 120 ^oC, synthesized nanoparticles were the mixture of Ce^{3+} and Ce^{4+}. Existence of Ce^{3+} forms bulk particles and prevents formation of the desired Ce^{4+} crystal. This phenomenon is shown in Figure 3.17. in presence of 8M RbOH alkali base.

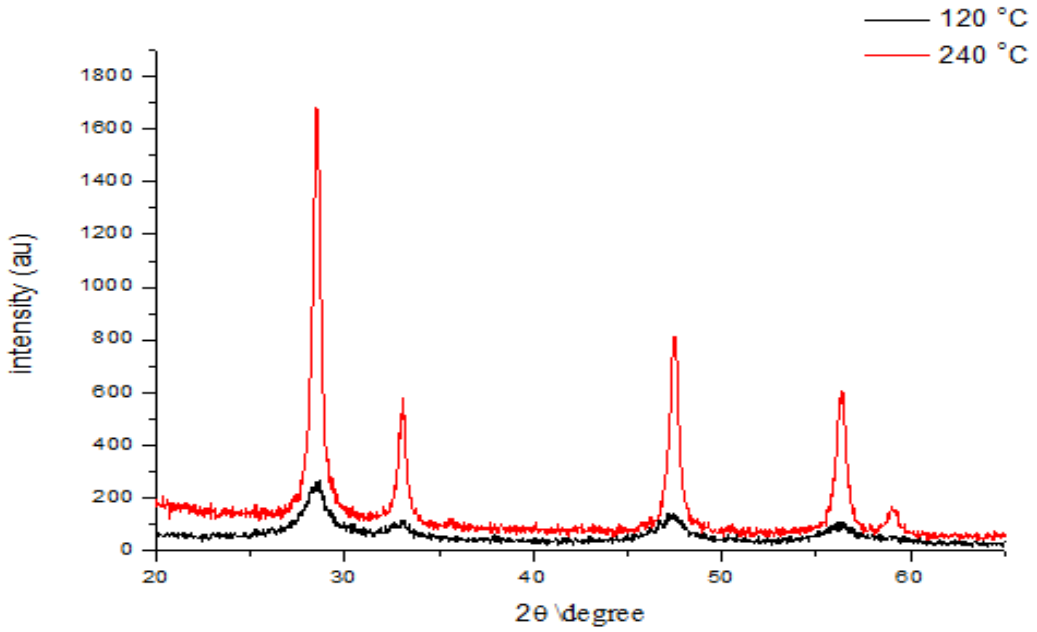

Figure 3.17. XRD patterns of CeO_2 nanoparticles in presence of RbOH under different reaction temperatures.

3.3. Optical Properties of CeO_2 Nanoparticles

The optical properties nanocrystallines have been studied in recent years. Considerable research has been focused on the fluorescence properties of nanomaterials because fluorescence may reveal the presence of crystalline defects resulting from the synthesis process. All absorbance and fluorometry measurements were done with the particles suspended in deionized water. Because of the low dispersibility of CeO_2 nanoparticles in water, dispersions were ultrasonically agitated for 10 min.

3.3.1. UV-Vis Spectroscopy

Figure 3.18 shows the absornbance spectrum of the cerium oxide nanoparticles synthesizde in the presence of 8M CsOH and 8M RbOH at 240 ^oC and 24 hours. The concentration of dispersions was 0.58 mM for both samples. When moving down the 1A group in the periodic table blue shift occurs in the absorbance values which means particle size decreases. Due to quantum confinement effect, the energy between lowest excitated state and ground state deals with the particle size. The smaller particle size, the

higher energy it has. Also the energy is reversely proportional with the wavelength. As a conclusion smaller particle sized nanoparticles have lower wavelength. (Deshpande, et al. 2005, Chai, et al. 2001, Tsunekawa, et al. 2000). Based on this phenomenon nanoparticles in presence of RbOH has larger particle size than CsOH.

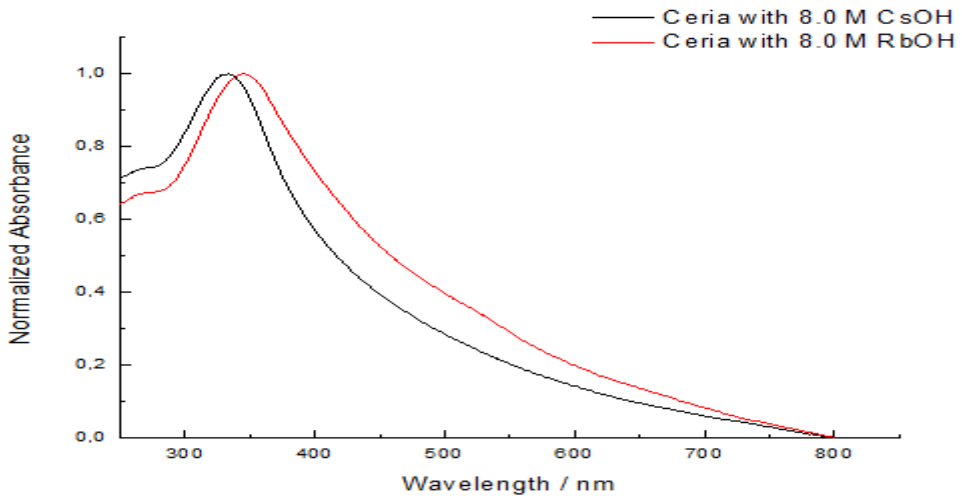

Figure 3.18. UV-Vis Spectra of CeO_2 nanoparticles in presence of CsOH and RbOH.

3.3.2. Fluorescence Spectroscopy

CeO_2 nanoparticles, synthesized in the presence of RbOH and CsOH at various temperature and reaction times suspended in H_2O and their photoluminescence emission spectrum recorded in this part of the study. The emission spectra of the CeO_2 nanoparticles measured at excitation wavelength of 270 nm, show two signals at 420 nm and 370 nm. The second signal at 420 nm can be attributed to the band-edge excition annihilation whereas the reason of the first signal at 370 nm is the substitutional defect (Ce^{3+}) in the crystal structure.

First of all, phototoluminescence of cerium oxide nanoparticles that were synthesized at different reaction temperatures was observed. As a generel truth Ce(III) defect states are considered as hexagonal crystal phase. Increasing temperature favors the face-centered cubic crystal structure to hexagonal crystal structure. Theoretical calculations show that face centered cubic phase is thermodynamically stable.

Therefore, the tendency towards the face centered cubic crystal structure with increasing temperature leads to a decrease in defect sites at higher temperatures (Im and Park 2002).

Figure 3.19. shows normalized emission of the particles. It was expected that the Ce^{3+} defect should be larger at 120 ^{o}C but nanoparticles synthesized at 120 ^{o}C were the mixture of green pulver Ce^{3+} and pure yellow Ce^{4+}. The Ce^{3+} does not behave as a defect there. Because of the existence itself, it may provide formation of the first signal at 370 nm.

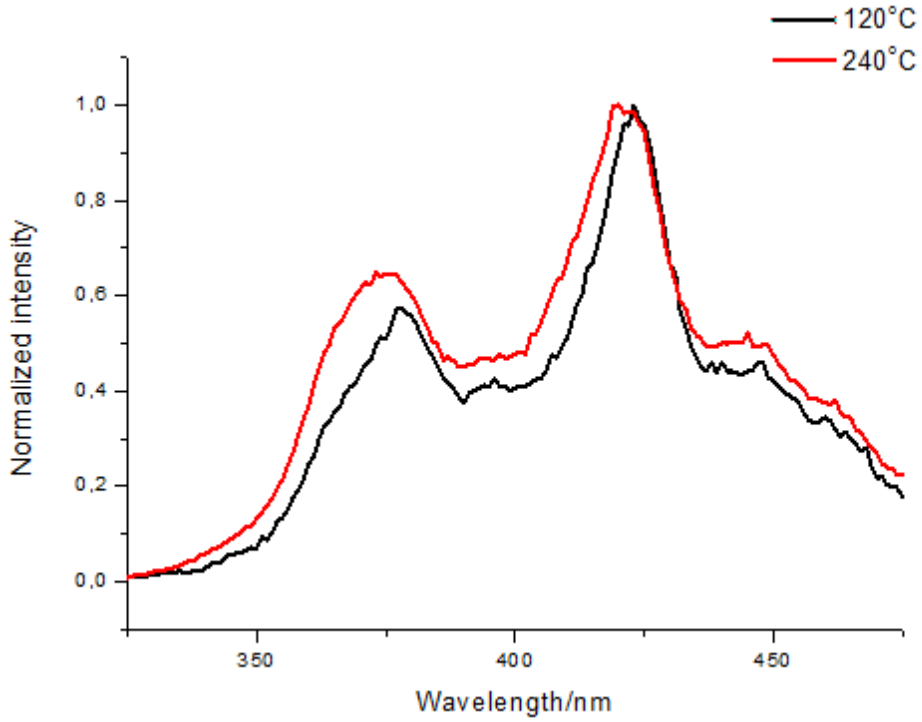

Figure 3.19. Room temperature fluorescence spectra of the CeO_2 nanoparticle dispersions at different reaction temperatures for 24 h.

Effect of reaction time on fluorescence spectrum of CeO_2 nanoaprticles in presence of 8M CsOH was investigated. As it is illustrated in Figure 3.20. 24 h. reaction time improves nucleation and crystall growth and as a result number of defects is reduced. Reactions at 1h. and 12h. show no significant difference in their spectrum but their defects are obviously larger than 24h.

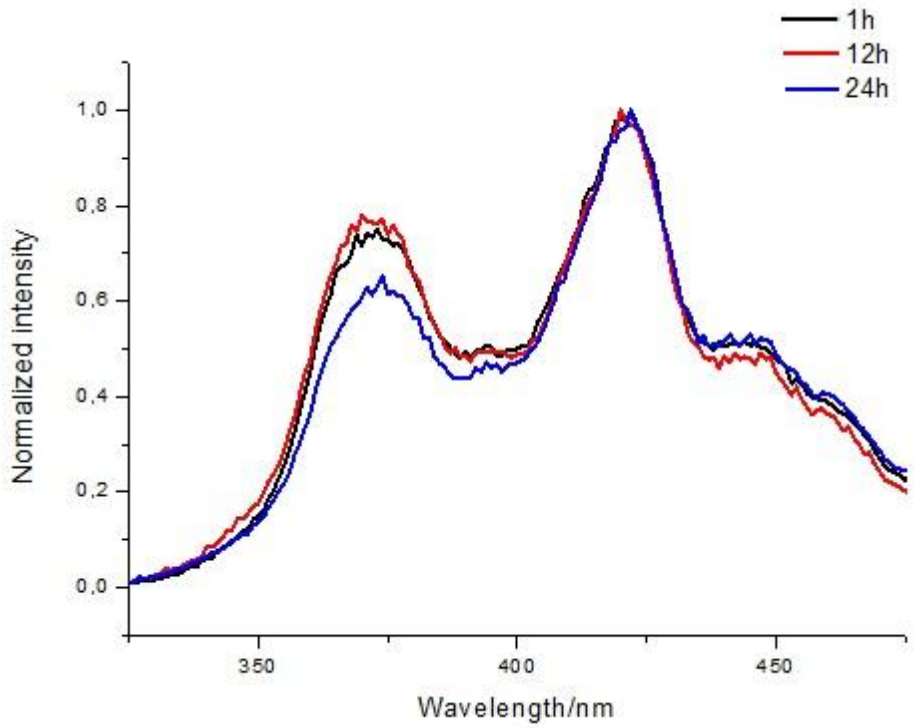

Figure 3.20. Room temperature fluorescence spectra of the CeO_2 nanoparticles in presence of 8M CsOH dispersions for different reaction times at 240°C.

When alkali effect on fluorescence spectrum is investigated, CeO_2 nanoparticles synthesized in presence of CsOH and RbOH shows no significant change Figure 3.21.

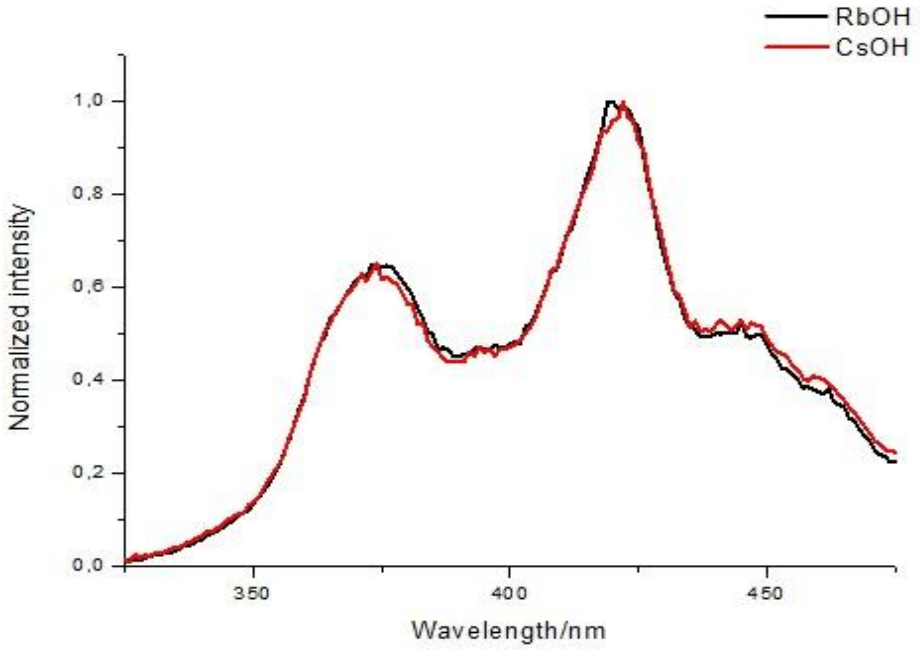

Figure 3.21. Room temperature fluorescence spectra of the CeO_2 nanoparticle dispersions with different alkali bases.

3.4. Catalytic Property of CeO_2 Nanoparticles

In this last part of the study the catalytic properties of cerium oxide nanoparticles were investigated. In 2006, Ahmad et al. synthesized 3',4',5,7-tetramethoxyflavone from 3,4,4',6'-tetramethoxychalcone. In order to achieve the synthesize, SeO_2 was used as a catalyst (Ahmad, et al. 2006) shown in Figure 3.22.

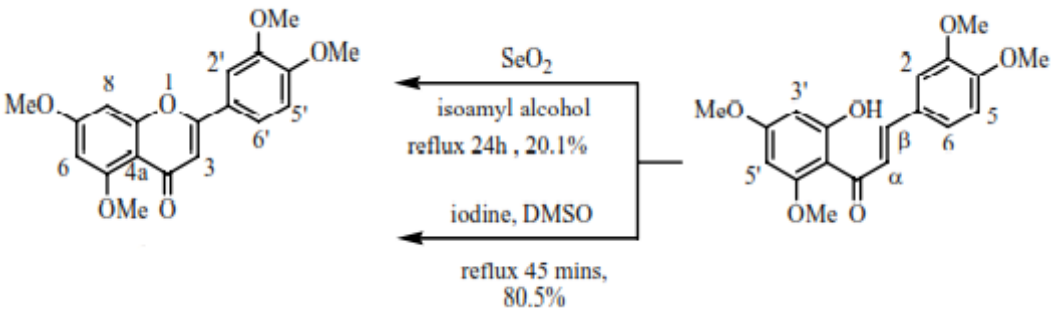

Figure 3.22. Transformation of 3,4,4',6'-tetramethoxychalcone to 3',4',5 tetramethoxyflavone in presence of SeO_2

We inspired from the study of Ahmad et al. and used CeO_2 nanoparticles instead of SeO_2 to determine whether the same transformation reaction occurs or not. The expected reaction is illustrated in Figure 3.23. In the firs step, a base catalyzed transformation of chalcones **(1)** into flavanones **(2)** was aimed and in the second step produced flavanones will be oxidized to corresponding flavones **(3)** in the presence of CeO_2 nanoparticles. Preliminary studies were performed in different solvents and temperatures. The results of these trials were summarized in Table 3.3. As it is shown in table, nanoparticles were tested in two forms; basic or neutral surfaces. The reactions were monitored by TLC, GC-MS and GC, and products were characterized by NMR spectroscopy.

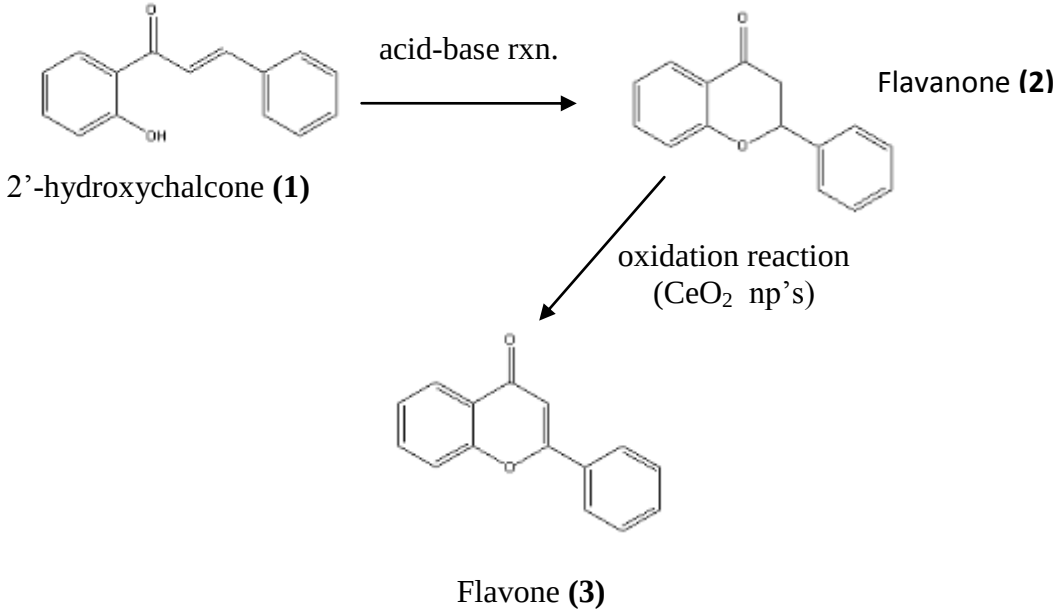

Figure 3.23. Synthesis of flavone **(3)** from 2'-hydroxychalcone **(1)**.

It seems temperature is critical for the formation of flavones. Although NaOH can't catalyze the reaction itself, NaOH treated CeO_2 can catalyze the reaction to give target product in low yields (Table 3.3., entries 2,4,6). Neutral CeO_2 nanoparticles are not effective catalyst for such transformation but NaOAc suprisingly yields the formation of flavone somehow in low yields.

Table 3.4. Reaction conditions for the synthesis of flavone **(3)** from 2'-hydroxychalcone **(1)**

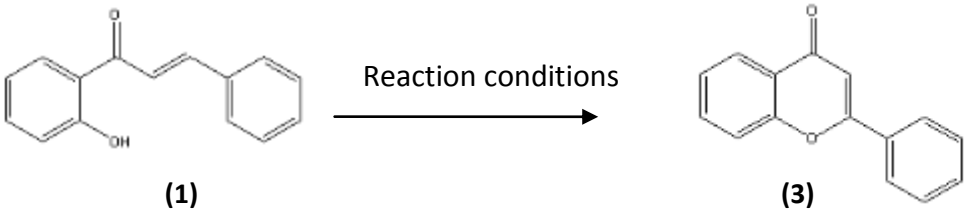

(1) **(3)**

Experiment[a]	**Chalcone(1) (1.3mmol)**	**Solvent (10ml)**	**Rxn. Temp. ^{o}C**	**Base (10%)**	**CeO_2 (0.1M RbOH) (30mg)**	**Yield (%)**[c]
1	2'-hydroxychalcone	DMSO	100	Sodium Acetate	-------	23
2[b]	2'-hydroxychalcone	DMSO	100	NaOH	-------	0
3[b]	2'-hydroxychalcone	DMSO	100	-------	Pure CeO_2	0
4	2'-hydroxychalcone	DMSO	100	--------	Treated CeO_2 with NaOH	30
5	2'-hydroxychalcone	DMF	100	Sodium Acetate	-------	16
6	2'-hydroxychalcone	DMF	100	----------	Treated CeO_2 with NaOH	20
7[b]	2'-hydroxychalcone	Ethanol	reflux	Sodium Acetate	--------	0
8[b]	2'-hydroxychalcone	Ethanol	reflux	Sodium Acetate	Pure CeO_2	0

[a] reaction time=24h. [b] complete recovery of reactant [c] isolated yield

In literature, it was reported that flavones **(3)** can be prepared from 1,3-dicarbonyl **(5)** compounds by treating with NaOAc (Ganguly, et al. 2005). To investigate the possible transformation unsubstituted chalcone **(4)** to corresponding 1,3-dicarbonyl species **(5)**. A set of experiments were designed as illustrated in Table 3.4. Unsubstituted chalcones **(4)** were treated with NaOAc or CeO_2 in DMF at 100 ^oC but there were no sign for the formation of such 1,3-dicarbonyl species.

Table 3.5. Results of the synthesis with unsubstituted chalcone **(4)** as a reactant.

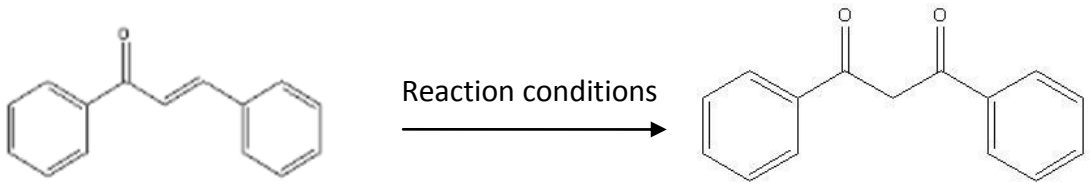

(4) **(5)**

Experiment[a]	**Chalcone (4) (1.3mmol)**	**Solvent (10ml)**	**Rxn. Temp. ^oC**	**Base (10%)**	**CeO_2 (0.1M RbOH) (30mg)**	**Yield (%)**[c]
9[b]	chalcone	DMF	100	Sodium Acetate	-------	0
10[b]	chalcone	DMF	100	----------	Treated CeO_2 with NaOH	0

[a] reaction time=24h. [b] complete recovery of reactant [c] isolated yield

CHAPTER 4

CONCLUSION

Cerium oxide nanoparticles were synthesized with hydrothermal method. XRD and SEM spectroscopic methods were used in order to characterize synthesized particles. This study is divided in to three parts. In the first part of the study effect of alkali type and concentration, reaction temperature and reaction time on morphology of cerium oxide nanoparticles were determined.

CsOH and RbOH alkali bases were chosen in order to synthesize nanoaprticles. Alkali concentration has strong influence on formation of nanoparticles. As the concentration of the base is increased the size of the nanoparticles increased on the other hand the average crystallite size decreased. Reaction temperature also has strong effect on the morphology. Increasing reaction temperature transforms cerium oxide nanoparticles in to cubic shape. When the reaction temperature is increased from 120 ^{o}C to 240 ^{o}C the rod-like particles transforms in to cubic nanoparticles. The reason for that is when the temperature is increased precipitated amorphous ceria dissolve in water and at the nucleation step, concentration of ceria monomers increased and recrystallized into nuclei.

Reaction time was also studied and 1, 12 and 24h. studies were completed. 24h. is the optimum time for obtaining single crystalline cubic CeO_2 nanoparticles. Shorter reaction times causes aggregated nanoparticles and increasing reaction time provides larger nanoparticles to form on the Ostwald ripening process.

Further studies dealed with optical properties of Cerium oxide nnaoparticles. Series of analysis were made with UV-VIS Spectrometry and Fluorescence Spectrometry. Based on the UV-VIS studies nanoparticles in the presence of RbOH alkali base have larger particle size than that of CsOH. Fluorescence spectra of nanoparticles at different reaction time shows that Ce^{+3} defect on particles is reversly proportional with time. When different alkali bases and reaction temperatures were compared there weren't any significant differences on their spectra.

In the last part of the study, catalytic properties of CeO_2 nanoparticles were investigated by using them as a catalyst in the synthesis of flavone starting from

2’-hydroxychalcone. Reaction parameters have been changed in order to achieve the formation of flavone. When different solvents were used and the other parameters were fixed, the rection favors to desired product in the presence of DMSO and DMF but not in ethanol. There may be two reasons for that. One of them is the solvent type that protic solvents (ethanol) are not appropriate for this reaction. The other one is reaction temperature. In the presence of ethanol we set up reflux system and that reflux temperature may not provide required activation energy for transformation of flavone. Additives were also changed and it was seen that the transformation did not complete in the presence of NaOH on the other hand, Sodium Acetate and treating CeO_2 nanoparticles with NaOH favors the formation of the desired product.

REFERENCES

Ahmad, F., Idrıs, M.S.H, Adıb, A.B., 2006. Synthesis and characterization some flavanoids derivatives. Department of Chemistry Faculty of Science. Universiti Teknologi Malaysia. Unpublished.

Barrer, R.M. 1948. Syntheses and reactions of mordenite. *Journal of Chemical Society*.2158.

Byrappa, Kullaiah, and Masahiro Yoshimura, eds. 2001. *Handbook of Hydrothermal Technology, A technology for Crystal Growth and Material Processing*. Noyes, New Jersey.

Byrappa, K. and Adschiri, T. 2007. Hydrothermal technology for nanotechnology. *Progress in Crystal Growth and Characterization of Materials*. 53:117-166.

Cabrera, M., Simoens, M., Falchi, G., Lavaggi, M. L., Piro, O. E., Castellano, E. E., Vidal, A., Azqueta, A., Monge, A., de Cerain, A. L., Sagrera, G., Seoane, G., Cerecetto, H. and Gonzalez, M. 2007. Synthetic chalcones, flavanones, and flavones as antitumoral agents: Biological evaluation and structure–activity relationships. *Bioorganic & Medicinal Chemistry* 15:3356–3367.

Calloway N. O.; Green L. D. 1937. Reactions in the Presence of Metallic Halides. I. – Unsaturated Ketone Formation as a Side Reaction in Friedel-Craft Acylations. *J. Am. Chem*. Soc. 59, 809–811.

Campbell, C.T. and Peden, C.H.F. 2005. Oxygen vacancies and catalysis on ceria surfaces. *Science*. 309:713-714.

Cao, Guohong. 2004. *Nanostructures and Nanomaterials*. Singapore: World Scientific Publishing Company.

Cermak R. 2008. "Effect of dietary flavonoids on pathways involved in drug metabolism". *Expert Opin Drug Metab Toxicol* 4 (1): 17–35.

Chai, C., Yang, S., Liu, Z., Liao, M., Chen, N., Wang, Z. 2005. The PL "violet shift" of cerium dioxide on silicon. *Chinese Science Bulletin*. 46:2046-2048(24).

Chen, P.L. and Chen, I.W. 1993. Reactive Cerium(IV) oxide powders by the homogeneous precipitation method. *Journal of American Ceramic Society*.76:1577-1583(6).

Cullity, B.D. 1978. *Elements of X-ray Diffraction*. Massachusetts: Addison-Wesley Publishing Company.

Deshpande, S., Patil, S., Satyanarayana, K., Seal, S. 2005. Size dependency variation in lattice paramater and valency states in nanocrystalline cerium oxide. *Applied Physics Letters*. 87:133113(3pp).

Dyke, S.F.; Ollis, W.D; Sainsbury, M.J. 1961. *Organic Chemistry* 26, 2453

Ganguly, A. K., Kaur, S., Mahata, P. K., Biswas, D., Pramanik, B. N. and Chan T.M. 2005. *Tetrahedron Letters*. 46: 4119- 4121.

Gormleg, T.R., O'Sullivan, W.I. 1973. *Tetrahedron* 29, 369

Goranson, R.W. 1931. Solubility of water in granite magmas. *American Journalof Science*. 22:481-502.

Han, W.Q., Wu, L., Zhu, Y. 2005. Formation and oxidation state of CeO2 nanotubes. *J. Am. Chem. Soc.* 127 (37), 12814-12815.

Im, S.H. and Park, O.O. 2002. Effect of evaporation temperature on the quality of colloidal crystals at the water-air interface. *Langmuir*. 18:9642-9646(25).

Imanaka, N., Masui, M., Hirai, H., Adachi, G. 2003. Amorphous cerium-titanium solid solution phosphate as a novel family of band gap tunable sunscreen materials. *Chemistry of Materials*. 15:2289-2291(12).

Iranpoor, N.; Kazemi, F. 1998. RuCl3 Catalyses Aldol Condensations of Aldehydes and Ketones. *Tetrahedron*, 54, 9475–9480.

Kalinin, A. V.; Da Silva, A. J. M.; Lopes, C. C.; Lopes, R. S. C.; Snieckus, V. 1998."Directed ortho metalation - cross coupling links. Carbamoyl rendition of the baker-venkataraman rearrangement. Regiospecific route to substituted 4-hydroxycoumarins". *Tetrahedron Lett.* 39 (28): 4995–4998.

Kang, Suk-Joong L. 2005. *Sintering – Densification, Grain Growth & Microstructure*. Butterworth-Heinemann.

Kaya, C., He, J.Y., Gu, X., Butler, E.G. 2002. Nanostructured ceramic powders by hydrothermal synthesis and their applications. *Microporous and Mesoporous Materials*. 54:37-49.

Kazauki, K., Htayama K., Yokomor, S., Soki, T. 1976 *Chem. Abstr.*, 85, 5913.

Kepenekçi, Ö., Emirdag-Eanes, M., Demir, M. M. Effect of Alkali Metal Hydroxides on the Morphological Development and Optical Properties of Ceria Nanocubes under Hydrothermal Conditions. *J. Nanosci. and Nanotechnol*. 11(4), 3565-3577, 2011.

Khodadadi, A., Mohajerzadeh, S.S., Mortazavi, Y., Miri, A.M. 2001. Cerium oxide/SnO_2 based semiconductor gas sensors with improved sensitivity to CO. *Sensors and Actuators B*. 80:267-271.

Komarneri, S. 2003. Nanophase materials by hydrothermal, microwave-hydrothermal and microwave-solvothermal methods. *Special Section: Nanoscience and Nanotechnology*. 85:1730-1734(12).

Kosynkin, V.D., Arzgatkina, A.A., Ivanov, E.N., Chtoutsa, M.G., Grabko, A.I., Kardapolov, A.V., Sysina, N.A. 2000. The study of process production of polishing powder based on cerium dioxide. *Journal of Alloys and Compounds*. 303:421-425.

Laudise, Robert A. 1970. *The Growth of Single Crystals*. Prentice Hall: Englewood Cliffs, NJ.

Lian, H., Zhang, M., Liu, J., Ye, Z., Yan, J., Shi, C. 2004. Synthesis and spectral properties of lutetium-doped CeF3 nanoparticles. *Chemical Physics Letters*. 395:362-365.

Mazza, L.; Guaram, A. 1980. An Improved Synthesis of 1,3-Diphenyl-2-buten-1-ones (-Methylchalcones). Synthesis, 41–44.

Nacken, R. 1946. Artificial quartz crystals. *U.S. Office of Technical Services Report* 18-28.

Nanoscienceworks 2012. Fabrication of nanomaterials. http://www.nanoscienceworks.org/publications/books/4/9781420048056/ITNS-STUDYGUIDE-Chap4-Fabrication.pdf. (accessed May 10, 2012).

Paul, B.K. and Moulik, S.P. 2001. Uses and applications of microemulsions. *SoftCondensed Matters*. 80:990-1001.

Peng, X. 2003. Mechanisms for the shape-control and shape-evolution of colloidal semiconductor nanocrystals. *Advanced Materials*. 15:459-463(5)

Rabenau, A. 1985. The role of hydrothermal synthesis in preparative chemistry. *Angew Chem (English Ed.)*. 24:1026-1040.

Rao, G.R., Mishra, B.G. 2003. Structural, redox and catalytic chemistry of ceria based materials. *Bulletin of the Catalysis Society of India*. 122-134.

Roy, R. 1994. Acceleration the kinetics of low-temperature inorganic syntheses. *Journal of Solid State Chemistry*. 111:11-17.

Sathyamurthy, S., Leonard, K.J., Dabestani, R.T., Paranthaman, M.P. 2005. Reverse micellar synthesis of cerium oxide nanoparticles. *Nanotechnology*. 16:1960-1964.

Schubert, Ulrich. and Nicola Hüsing, eds. 2000. *Synthesis of Inorganic Materials*. Weinheim, Germany: Wiley-WCH

Shimadzu 2012. GC. http://www.shimadzu.com/an/gc/index.html. (accessed July 10, 2012).

Skoog, D.A., Holler, F.J., Nieman, T.A. 1998. *Principles of Instrumental Analysis*. USA: Brooks/Cole Thomson Learning.

Smart, Lesley and Elaine A. Moore, eds. 1996. *Solid State Chemistry – An Introduction*. Cheltenham: Stanley Thornes

Strobel, A.S. and Heineman, R.W. 1989. *Chemical Instrumentation: A Systematic Approach.* New York: John Wiley & Sons, Inc.

Tsunekawa, S., Fukuda, T. and Kasuya, A. 2000. Blue shift in ultraviolet absorption spectra of monodisperse CeO2-x nanoparticles. *Journal of Applied Physics*. 87:1318-1321(3).

Wade, L.G. 2009. *Organic Chemistry* 7th. ed. USA: Prentice Hall.

Wang, H., Zhu, J.J., Zhu, J.M., Liao, X.H., Xu, S., Ding, T., Chen, H.Y. 2002.Preparation of nanocrystalline ceria nanoparticles by sonochemical and microwave assisted heating methods. *Physical Chemistry Chemical Physics*. 4:3794-3799.

Wang C. H., Lin S. S., 2004. Preparing an active cerium oxide catalyst for the catalytic incineration of aromatic hydrocarbons. *Appl. Catal*. A 268227-233.

Wikipedia contributors, "Transmission Electron Microscopy". 2007e. Wikipedia, The Free Encyclopedia. http://en.wikipedia.org/wiki/Transmission_electron_microscopy (accessed June 20, 2012).

Wu, G.S., Xie, T., Yuan, X.Y., Cheng, B.C., Zhang, L.D. 2004. An improved solgel template synthetic route to large scale CeO_2 nanowires. *Materials Research Bulletin*. 39:1023-1028.

Yan, Z.G. and Yan, C.H. 2008. Controlled synthesis of rare earth nanostructures. *Journal of Materials Chemistry*. 18:5046-5059.

Yang, Z., Zhou, K., Liu, X., Tian, Q., Lu, D., Yang, S. 2007. Single-crystalline ceria nanocubes: Size controlled synthesis, characterization and redox property. *Nanotechnology*. 18:185606(4pp).

Yin, L., Wang, Y., Pang, G., Koltypin, Y., Gedanken, A. 2002. Sonochemical synthesis of cerium oxide nanoparticles-Effect of additives and quantum size effect. *Journal of Colloid and Interface Science*. 246, 78-84.

Zhang, T., Hing, P., Huang, H., Kilner, J. 2002. Sintering study on commercial CeO_2 powder with small amount of MnO_2 doping. *Materials Letters*. 57:507-512.

Zhang, T.S., Ma, J., Kong, L.B., Zeng, Z.Q., Hing, P., Kilner, J.A. 2003. Final-stage sintering behavior of Fe-doped CeO_2. *Materials Science and Engineering B.*103:177-183.

Zhang, J., Ju, X., Wu, Z.Y., Liu, T., Hu, T.D., Xie, Y.N. 2001. Structural characteristics of cerium oxide nanocrystals prepared by the microemulsion method. *Chem. Mater*. 13, 4192-4197

Zhou, X.D., Huebner, W. and Anderson, H.U. 2002. Room temperature homogeneous nucleation synthesis and thermal stability of nanometer single crystal CeO_2. *Applied Physics Letters*. 80:3814-3816(20).

Zubick, J.W. 1988. Organic Chem. Lab Survival Manual. *A Students Guide to Techniques.* USA: John Wiley & Sons, Inc.

APPENDIX A

^{1}H NMR SPECTRUM OF UNSUBSTITUTED CHALCONE

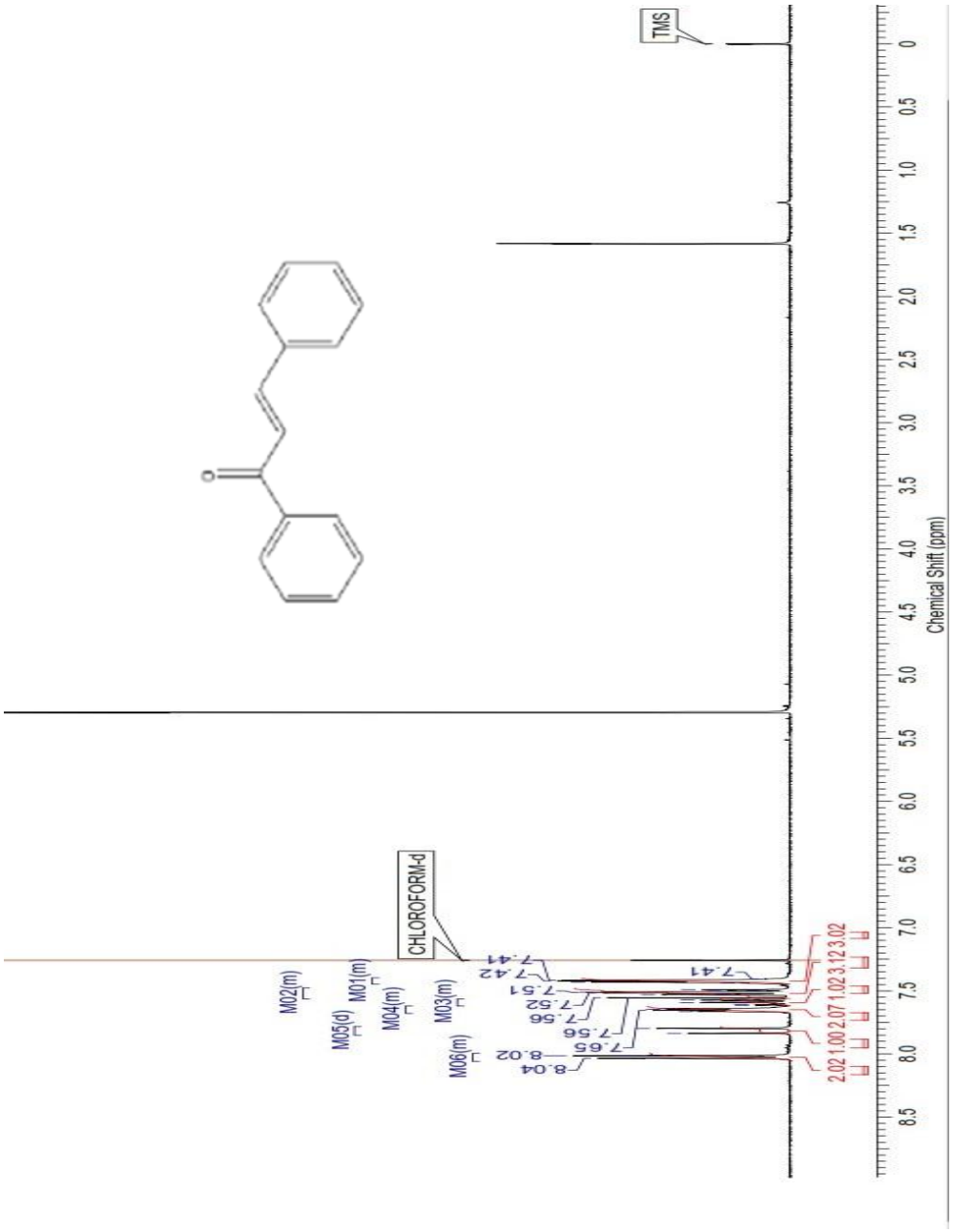

Figure A.1. ^{1}H NMR spectrum of unsubstituted chalcone

APPENDIX B

GC SPECTRUM OF UNSUBSTITUTED CHALCONE

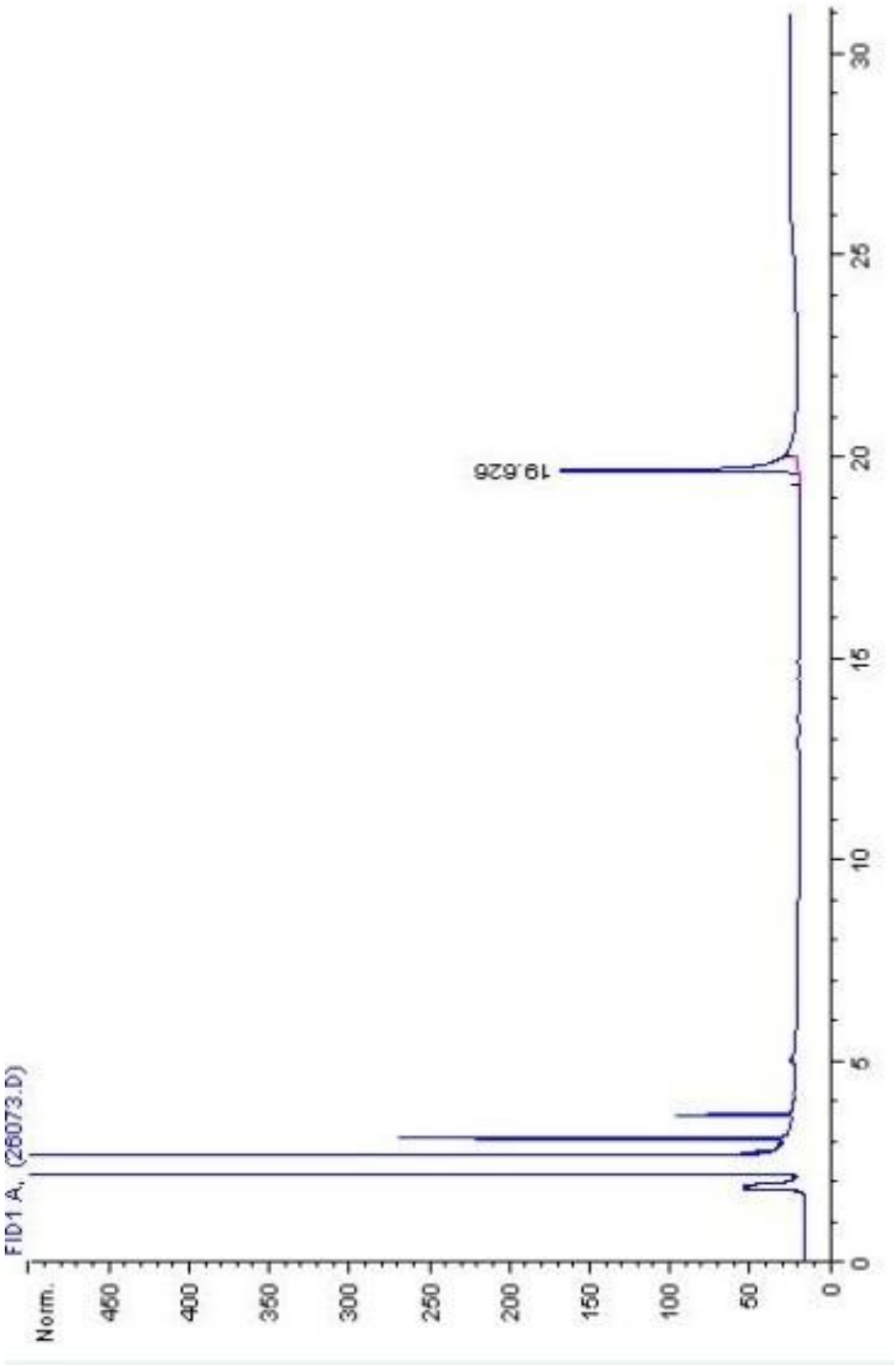

Figure B.1. GC spectrum of unsubstituted chalcone

APPENDIX C

GC-MS SPECTRUM OF UNSUBSTITUTED CHALCONE

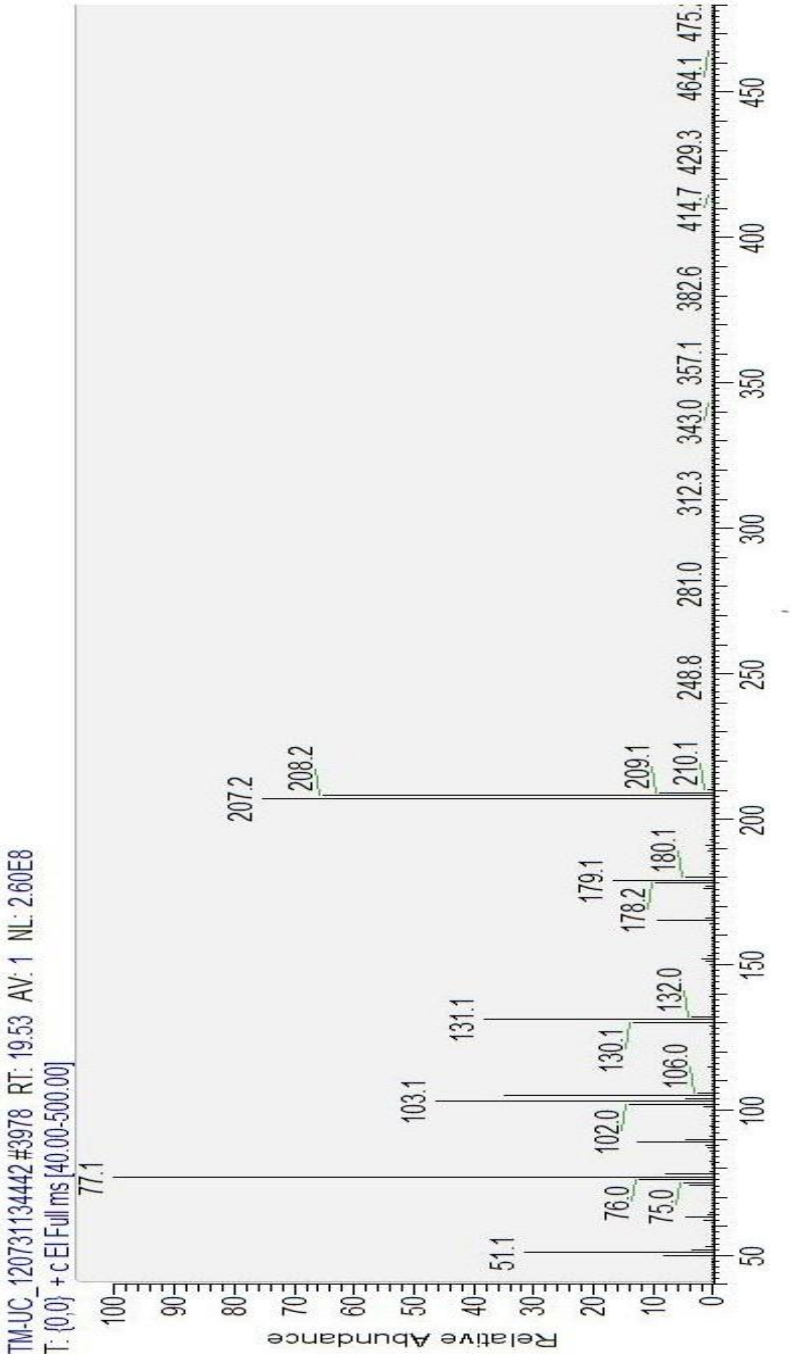

Figure C.1. MS spectrum of unsubstituted chalcone

APPENDIX D

NMR SPECTRUM OF FLAVONE

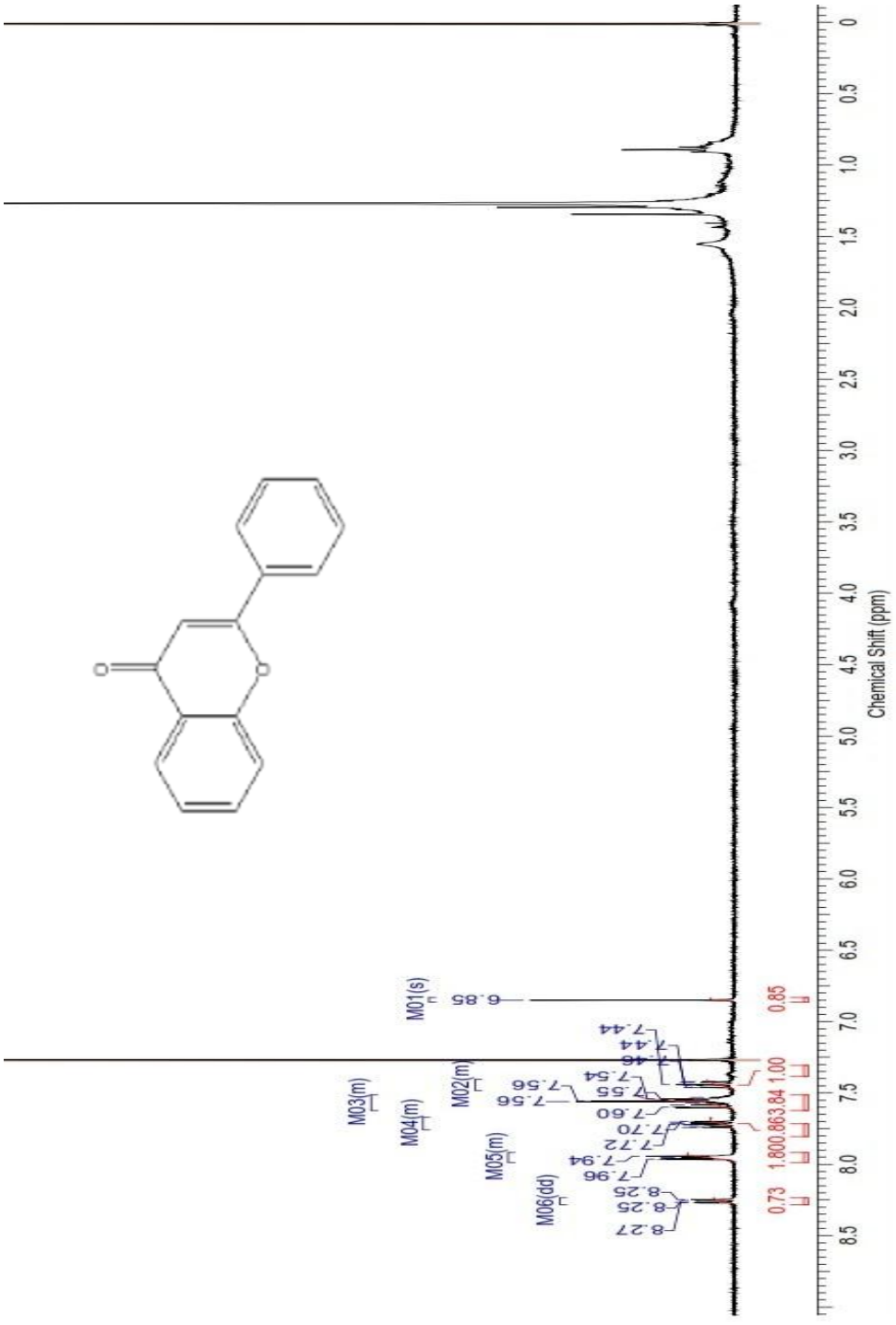

Figure D.1. ^{1}H NMR spectrum of flavone

APPENDIX E

GC SPECTRUM OF FLAVONE

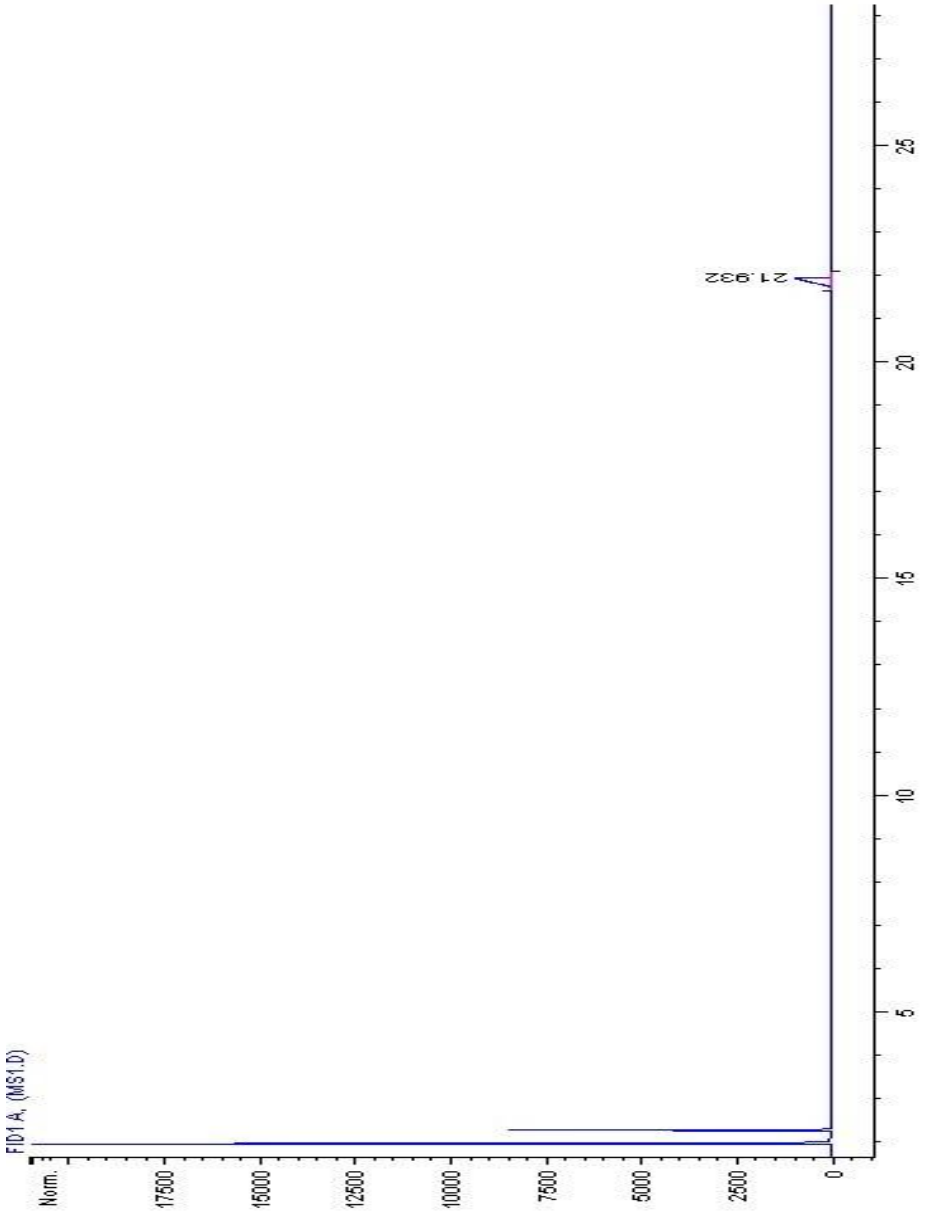

Figure E.1. GC spectrum of flavone

APPENDIX F

MASS SPECTRUM OF FLAVONE

Figure F.1. MS spectrum of flavone